Available online at www.sciencedirect.com

ScienceDirect

Journal of the Franklin Institute 356 (2019) 3474–3507

www.elsevier.com/locate/jfranklin

Spacecraft formation flying reconfiguration with extended and impulsive maneuvers

G. Di Mauro[a], D. Spiller[b], R. Bevilacqua[a,*], S. D'Amico[c]

[a] *Department of Mechanical and Aerospace Engineering, Advanced Autonomous Multiple Spacecraft (ADAMUS) Laboratory, University of Florida, 939 Sweetwater Dr., Gainesville, FL 32611-6250, USA*

[b] *Department of Aerospace and Mechanical Engineering, Sapienza University of Rome, via Eudossiana 18,00100, Italy*

[c] *Department of Aeronautics and Astronautics Engineering, Space Rendezvous Laboratory, Stanford University, 496 Lomita Mall, Stanford, CA 94305-4035, USA*

Received 28 August 2017; received in revised form 7 November 2018; accepted 4 February 2019
Available online 26 February 2019

Abstract

This paper presents the control solutions to the spacecraft formation reconfiguration problem when impulsive or extended maneuvers are considered, and the reference orbit is circular. The proposed approach for the derivation of the control solutions is based on the inversion of the linearized equations of relative motion parameterized using the mean relative orbit elements. The use of mean relative orbit elements eases the inclusion of perturbing accelerations, such as the Earth's oblateness effects, and offers an immediate insight into the relative motion geometry. Several maneuvering schemes of practical operational relevance are considered and the performance of the derived impulsive and piecewise continuous control solutions are investigated through the numerical propagation of the nonlinear relative dynamics. Finally, the benefits of the new extended maneuvers strategies are assessed through a comparison with the corresponding impulsive one.
© 2019 The Franklin Institute. Published by Elsevier Ltd. All rights reserved.

1. Introduction

Spacecraft formation flying has received great attention in last two decades thanks to the advantages it offers in terms of costs, mission flexibility/robustness, and enhanced per-

* Corresponding author.
E-mail addresses: gdimauro@ufl.edu (G. Di Mauro), bevilr@ufl.edu (R. Bevilacqua).

https://doi.org/10.1016/j.jfranklin.2019.02.012
0016-0032/© 2019 The Franklin Institute. Published by Elsevier Ltd. All rights reserved.

formance [1,2]. In fact, the distribution of tasks and payload among multiple cooperative spacecraft gives the opportunity to overcome the limitations due to using a single satellite system for the mission goal accomplishment. Among the various technical challenges involved in spacecraft formation flying, the design of control laws for reconfiguration represents a key aspect that has been intensively studied over the last years. The reconfiguration problem pertains to the achievement of a specific relative orbit in a defined time interval given an initial formation configuration. So far, many methods have been proposed to solve the aforementioned problem, ranging from the impulsive to the continuous control techniques, [3]. Impulsive strategies have been widely investigated since they provide an analytical solution to the relative motion control problem. Such solutions are generally based on (1) the use of the Gauss Variational Equations (GVE), to determine the control influence matrix, and (2) on the inversion of the state transition matrix (STM) associated with a set of linear equations of relative motion. Vaddi et al. [1] addressed the issues of establishment and reconfiguration of a multiple spacecraft formation, consisting of a central chief satellite surrounded by four deputy spacecraft, for unperturbed orbits using impulsive control. They proposed an analytical two-impulse control scheme for transferring a deputy spacecraft from a given location in the initial configuration to any given final configuration, using the GVE. Ichimura et al. [4] developed an analytical open-time minimum fuel impulsive strategy associated with the Hill-Clohessy-Wiltshire equations of relative motion. It involves three in-plane impulses to achieve the optimal in-plane reconfiguration. Gaias and D'Amico [3] addressed the problem of multi-impulsive solution schemes for formation reconfiguration in near-circular keplerian orbits using Relative Orbit Elements (ROE). They proposed a general methodology, based on the inversion of relative dynamics equations, which led to the straightforward computation of analytical or numerical control solutions. A similar impulsive approach based on the ROE parametrization is developed by Chernick et al. in [5]. Here, the authors extended the results reported in [3] deriving analytical and semi-analytical solutions for in-plane and out-of-plane reconfigurations, respectively, in near-circular perturbed and eccentric unperturbed orbits.

Planning continuous reconfiguration maneuvers is usually more challenging. However, continuous maneuvers might be necessary when spacecraft are equipped with low-thrust actuation systems. So far, many control approaches have been investigated. In [6] Armellin et al. derived the minimum-fuel formation reconfiguration maneuver using the sequential quadratic programming (SQP) method. To deal with the orbital perturbations a dynamic refresh of optimal trajectories computed by the aforementioned algorithm is done. The Gauss Pseudospectral Method (GPM) was employed in [7] whereas a two-stage path planning approach was used in [8], which combines a bi-directional Rapidly-exploring Random Tree (RRT) planner with a GPM. A continuous low-thrust control strategy for formations operating in perturbed orbits of arbitrary eccentricity was proposed by Steindorf et al. [9]. The authors derived a control law based on the Lyapunov theory and ROE dynamics parameterization, and implemented algorithms based on the potential fields for the guidance strategy. This approach allowed inclusion of the time constraint, thrust level constraint, wall constraints and passive collision avoidance constraint. Bae et al. [10] designed a controller for spacecraft formation flying using a sliding mode control scheme with the adaptive gain and neural networks. They considered a 6DOF spacecraft nonlinear dynamic model and adopted a leader-follower approach. Imani et al. [11] developed an optimal sliding mode controller based on the linearized two-body relative dynamics. The optimal control design was based on a linear quadratic method supplemented by an integral sliding mode control technique to robustify the controller. Di Mauro et al. [12] proposed a nonlinear controller based on State-Dependent Riccati Equation

(SDRE) technique to solve the coupled orbital and attitude relative motion control problem for a 2-satellite formation flying. Here the relative dynamics model used for the controller design included the J2 and drag perturbing effects. In [13] the 4-satellite formation reconfiguration problem is tackled as a coordination problem of a 3D second-order non-linear agents formation under a directed communication. The authors derived a control law for the relative motion by treating the coordinated orbit-tracking control model for each agent as a cascade system composed of orbit-tracking subsystem and the formation subsystem with the orbit-tracking error as input.

Some efforts have been done also to derive the analytical continuous solutions to the relative motion control problem. In [14] the authors determined the fuel-optimal analytical maneuvers using the Tschauner–Hempel model whereas in [15] the fuel-optimal analytical solutions are studied considering several linear relative dynamics models. The differential gravity effects, as well as the eccentricity and J2 effects are introduced in [16], while some special cases were taken into account in [17] and [18]. The former focused on projected circular orbits and the latter considered the Hill Three-Body Dynamics around the L2 Lagrangian point. All these works were based on the Cartesian description of the relative motion. More recently, Lawn et al. [19] proposed a continuous low-thrust strategy based on the input-shaping technique for the short-distance planar spacecraft rephasing and rendezvous maneuvering problems. The analytical solution was obtained by exploiting the Schweighart and Sedwick (SS) linear dynamics model. Finally, Larbi et al. [20] derived a control concept for far range formation flying applications based on ROE parameterization, assuming circular unperturbed reference orbits.

This paper addresses the derivation of analytical impulsive and piecewise continuous solutions for the control of spacecraft formation configuration. The analytical solutions are characterized by a high level of determinism and predictability and are suited for an onboard implementation, avoiding running computationally burdensome control numerical algorithms. In this study the relative motion is parameterized in terms of ROE taking into account the J_2 perturbation. In the framework of spacecraft relative motion, different dynamics models have been developed over the years, based on different state representation and subject to a multitude of constraints and limitations on the inter-satellite range of applicability, the eccentricity of the satellite orbits, and the type of modeled perturbation forces. For a comprehensive comparison among the different existing dynamics models we address the reader to [21,22].

The main contributions of this work are:

1. the development of a linearized relative dynamics model including the J_2 perturbation and the control accelerations and its associated closed-form solution, for near-circular reference orbits (see Section 2);
2. the derivation of impulsive and piecewise continuous solutions for in-plane and out-of-plane formation reconfiguration, taking into account the J_2 perturbation effects (see Section 3.2–3.3). In further details, starting from the approach presented in [5] and [23], 2- and 3-maneuver strategies are designed for in-plane reconfiguration, whereas a single maneuver approach is proposed for the out-of-plane maneuvering;
3. the comparison in terms of maneuvering cost and accuracy between the continuous and impulsive control schemes (see Section 4);
4. the development of a computationally efficient algorithm to modify the analytical 3-maneuver continuous control solution to be compatible with thrusters that operate in on/off configuration (see Section 4.1.1).

The rest of the paper is organized as follows. In Section 2, the nonlinear and linear dynamics models describing the relative motion of two Earth orbiting spacecraft under the effects of J_2 and continuous external accelerations are presented. The closed-form solution for the dynamics is determined for near-circular perturbed orbits, i.e. for very small or zero eccentricity. Section 3 details the mathematical formulation for control solutions through piecewise continuous and impulsive strategies for in-plane and out-of-plane reconfiguration maneuvering. The results are reported in Section 4, wherein relative trajectories obtained using the developed control laws are shown, pointing out their performances in terms of maneuver cost and accuracy. A comparisons between impulsive and continuous schemes is also carried out and detailed in the same section. Conclusions and final remarks are given in Section 5.

2. Relative dynamics model

In this section the dynamics model describing the relative motion between two Earth satellites and its associated closed-form solution is presented. The model is formulated using the dimensionless relative orbit elements defined by D'Amico in [24]. The developed linear model allows inclusion of the effects of Earth's oblateness, J_2, and those due to the external constant accelerations. Then, the findings in [25] are extended by computing the input matrix and the corresponding convolution matrix to count for the control acceleration provided by the deputy satellite.

2.1. Relative orbit elements

The relative motion of a satellite, referred to as *deputy*, with respect to another one, referred to as *chief*, can be parameterized using the following combination of classical keplerian orbit elements, $\boldsymbol{\alpha} = [a, e, i, \omega, \Omega, M]^T$,

$$\delta\boldsymbol{\alpha} = \begin{bmatrix} \frac{a_d}{a_c} - 1 \\ (M_d - M_c) + (\omega_d - \omega_c) + (\Omega_d - \Omega_c)c_{i_c} \\ e_{xd} - e_{xc} \\ e_{yd} - e_{yc} \\ i_d - i_c \\ (\Omega_d - \Omega_c)s_{i_c} \end{bmatrix} = \begin{bmatrix} \delta a \\ \delta\lambda \\ \delta e_x \\ \delta e_y \\ \delta i_x \\ \delta i_y \end{bmatrix} \tag{1}$$

known in literature as quasi-nonsingular relative orbit elements, [24,25]. In Eq. (1) the subscripts c and d stand for chief and deputy respectively, whereas $s_{(\cdot)} = \sin(\cdot)$ and $c_{(\cdot)} = \cos(\cdot)$. Moreover, $e_{x(\cdot)} = e_{(\cdot)}c_{\omega_{(\cdot)}}$ and $e_{y(\cdot)} = e_{(\cdot)}s_{\omega_{(\cdot)}}$ are the components of the eccentricity and ω is the argument of perigee. The first two elements of the relative state vector, $\delta\boldsymbol{\alpha}$, are the relative semi-major axis, δa, and the relative mean longitude, $\delta\lambda$, whereas the remaining components constitute the coordinates of the relative eccentricity vector, $\delta\boldsymbol{e}$, and relative inclination vector, $\delta\boldsymbol{i}$. Note that that the above state representation is non-singular for circular orbit ($e_c = 0$), whereas it is still singular for strictly equatorial orbit ($i_c = 0$). As the above parameterization is based on a combination of Keplerian orbital elements, it facilitates the inclusion of perturbing accelerations (e.g., Earth oblateness J_2 effects) into the dynamics model through the well-known GVE, [26,27]. Moreover, it offers an immediate insight into the relative motion geometry, [28].

2.2. Non-linear equations of relative motion

The averaged variations of mean ROE (i.e. without short- and long-periodic terms) caused by J_2 effects can be derived from the differentiation of chief and deputy mean classical elements, $\boldsymbol{\alpha}_c = [a_c, e_c, i_c, \omega_c, \Omega_c, M_c]^T$ and $\boldsymbol{\alpha}_d = [a_d, e_d, i_d, \omega_d, \Omega_d, M_d]^T$ respectively, [29,30],

$$\dot{\boldsymbol{\alpha}}_{c,J_2} = \begin{bmatrix} \dot{a}_c \\ \dot{e}_c \\ \dot{i}_c \\ \dot{\omega}_c \\ \dot{\Omega}_c \\ \dot{M}_c \end{bmatrix} = K_c \begin{bmatrix} 0 \\ 0 \\ 0 \\ Q_c \\ -2cos(i_c) \\ \eta_c P_c \end{bmatrix}, \quad \dot{\boldsymbol{\alpha}}_{d,J_2} = \begin{bmatrix} \dot{a}_d \\ \dot{e}_d \\ \dot{i}_d \\ \dot{\omega}_d \\ \dot{\Omega}_d \\ \dot{M}_d \end{bmatrix} = K_d \begin{bmatrix} 0 \\ 0 \\ 0 \\ Q_d \\ -2cos(i_d) \\ \eta_c P_d \end{bmatrix} \tag{2}$$

where

$$\begin{gathered} K_j = \frac{\gamma n_j}{a_j^2 \eta_j^4}\,, \ \eta_j = \sqrt{1-e_j^2}\,, \ n_j = \sqrt{\frac{\mu_\oplus}{a_j^3}}\,, \\ Q_j = 5cos(i_j)^2 - 1\,, \ P_j = 3cos(i_j)^2 - 1\,, \ \gamma = \tfrac{3}{4} J_2 R_E^2\,. \end{gathered} \tag{3}$$

In Eq. (3) the subscript j stands for c and d. J_2 indicates the second spherical harmonic of the Earth's geopotential ($J_2 = 1.082 \times 10^{-3}$), R_E the Earth's equatorial radius ($R_E = 6378.1363$ km) and $\mu_\oplus$ the Earth gravitational parameter ($\mu_\oplus = 398600.4415$ (km^3/s^2)). Computing the time derivative of mean ROE as defined in Eq. (1) and substituting Eq. (2) yields

$$\delta\dot{\boldsymbol{\alpha}}_{J_2} = \begin{bmatrix} 0 \\ \left(\dot{M}_d - \dot{M}_c\right) + \left(\dot{\omega}_d - \dot{\omega}_c\right) + \left(\dot{\Omega}_d - \dot{\Omega}_c\right) c_{i_c} \\ -e_d s_{\omega_d} \dot{\omega}_d + e_c s_{\omega_c} \dot{\omega}_c \\ +e_d c_{\omega_d} \dot{\omega}_d - e_c c_{\omega_c} \dot{\omega}_c \\ 0 \\ \left(\dot{\Omega}_d - \dot{\Omega}_c\right) s_{i_c} \end{bmatrix} = \boldsymbol{\sigma}_{J_2}(\boldsymbol{\alpha}_c, \boldsymbol{\alpha}_d) \tag{4}$$

with

$$\boldsymbol{\sigma}_{J_2}(\boldsymbol{\alpha}_c, \boldsymbol{\alpha}_d) = \begin{bmatrix} 0 \\ (\eta_d P_d K_d - \eta_c P_c K_c) + (K_d Q_d - K_c Q_c) - 2\left(K_d c_{i_d} - K_c c_{i_c}\right) c_{i_c} \\ -e_{yd} K_d Q_d + e_{yc} K_c Q_c \\ e_{xd} K_d Q_d - e_{xc} K_c Q_c \\ 0 \\ -2\left(K_d c_{i_d} - K_c c_{i_c}\right) s_{i_c} \end{bmatrix} \tag{5}$$

In this study only the deputy is assumed to be maneuverable and capable of providing a thrust along x, y, and z directions of its own Radial-Tangential-Normal (RTN) reference frame (also known as Local Vertical Local Horizontal (LVLH)). The RTN frame consists of a basis vectors with x pointing radially away from the Earth to the deputy satellite, z pointing along the direction of the angular momentum of the deputy orbit, and y completing the right-handed ortho-normal basis. The change of mean ROE caused by a continuous control acceleration vector $\boldsymbol{F}$ can be determined through the GVE [26,27]. In fact, the mean orbit elements can be reasonably approximated by the corresponding osculating ones as the Jacobian of the osculating-mean mapping is approximately a 6×6 identity matrix with the off-diagonal terms being of order J_2 or smaller, [27]. In light of this, the change in mean ROE due to an external

force is

$$\delta\dot{\boldsymbol{\alpha}}_F = \begin{bmatrix} \frac{\dot{a}_d}{a_c} \\ \dot{M}_d + \dot{\omega}_d + \dot{\Omega}_d c_{i_c} \\ \dot{e}_d c_{\omega_d} - e_d s_{\omega_d} \dot{\omega}_d \\ \dot{e}_d s_{\omega_d} + e_d c_{\omega_d} \dot{\omega}_d \\ \dot{i}_d \\ \dot{\Omega}_d s_{i_c} \end{bmatrix} = \boldsymbol{\sigma}_F(\boldsymbol{\alpha}_d, \boldsymbol{F}) = \boldsymbol{\Gamma}_F(\boldsymbol{\alpha}_d)\boldsymbol{F} \tag{6}$$

where the control acceleration vector $\boldsymbol{F}$ is expressed in the RTN frame components as $\boldsymbol{F} = [f_x, f_y, f_z]^T$. The individual terms of the control influence matrix $\boldsymbol{\Gamma}_F$ are reported in Appendix A, [9].

The relative motion between the deputy and the chief satellites is given adding the contributions of the point-mass gravitational field, the J_2 perturbation and the external force $\boldsymbol{F}$. The final set of nonlinear differential equations is

$$\begin{aligned} \delta\dot{\boldsymbol{\alpha}} &= [0, n_d - n_c, 0, 0, 0, 0]^T + \boldsymbol{\sigma}_{J_2}(\boldsymbol{\alpha}_c, \boldsymbol{\alpha}_d) + \boldsymbol{\sigma}_F(\boldsymbol{\alpha}_d, \boldsymbol{F}) \\ &= \boldsymbol{\xi}(\boldsymbol{\alpha}_c, \boldsymbol{\alpha}_d(\boldsymbol{\alpha}_c, \delta\boldsymbol{\alpha}), \boldsymbol{F}). \end{aligned} \tag{7}$$

Note that the function $\boldsymbol{\xi}(\boldsymbol{\alpha}_c, \boldsymbol{\alpha}_d(\boldsymbol{\alpha}_c, \delta\boldsymbol{\alpha}), \boldsymbol{F})$ can be reformulated in terms of $\boldsymbol{\alpha}_c$ and $\delta\boldsymbol{\alpha}$ using the following identities

$$\begin{aligned} a_d &= a_c \delta a + a_c\,, \;\; e_d = \sqrt{(e_c c_{\omega_c} + \delta e_x)^2 + (e_c s_{\omega_c} + \delta e_y)^2} \\ i_d &= i_c + \delta i_x\,, \;\; \omega_d = \tan^{-1}\left(\frac{e_c s_{\omega_c} + \delta e_y}{e_c c_{\omega_c} + \delta e_x}\right) \\ \Omega_d &= \Omega_c + \frac{\delta i_y}{s_{i_c}}\,, \;\; M_d = M_c + \delta\lambda - (\omega_d - \omega_c) - (\Omega_d - \Omega_c)c_{i_c}\,, \end{aligned} \tag{8}$$

such that $\delta\dot{\boldsymbol{\alpha}} = \boldsymbol{\xi}(\boldsymbol{\alpha}_c, \delta\boldsymbol{\alpha}, \boldsymbol{F})$.

2.3. Linearized equations of relative motion

In order to obtain the linearized equations of relative motion, $\delta\dot{\boldsymbol{\alpha}}$ in Eq. (7) can be expanded about the chief orbit (i.e., $\delta\boldsymbol{\alpha} = 0$ and $\boldsymbol{F} = 0$) to first order using a Taylor expansion,

$$\delta\dot{\boldsymbol{\alpha}}(t) = \left.\frac{\partial\boldsymbol{\xi}}{\partial\delta\boldsymbol{\alpha}}\right|_{\substack{\delta\boldsymbol{\alpha}=0 \\ \boldsymbol{F}=0}} \delta\boldsymbol{\alpha}(t) + \left.\frac{\partial\boldsymbol{\xi}}{\partial\boldsymbol{F}}\right|_{\substack{\delta\boldsymbol{\alpha}=0 \\ \boldsymbol{F}=0}} \boldsymbol{F}(t) = \boldsymbol{A}(\boldsymbol{\alpha}_c(t))\delta\boldsymbol{\alpha}(t) + \boldsymbol{B}(\boldsymbol{\alpha}_c(t))\boldsymbol{F}. \tag{9}$$

The matrices $\boldsymbol{A}$ and $\boldsymbol{B}$ represent the plant and input matrices respectively and are [9,29]

$$\boldsymbol{A} = \begin{bmatrix} 0 & 0 & 0 & 0 & 0 & 0 \\ -\Lambda_c & 0 & e_{xc}K_cG_cP_cF_c & e_{yc}K_cG_cP_cF_c & -K_cF_cS_c & 0 \\ \frac{7K_cQ_ce_{yc}}{2} & 0 & -4e_{xc}e_{yc}K_cG_cQ_c & -(1+4e_{yc}^2G_c)K_cQ_c & 5e_{yc}K_cS_c & 0 \\ -\frac{7K_cQ_ce_{xc}}{2} & 0 & (1+4e_{xc}^2G_c)K_cQ_c & 4e_{xc}e_{yc}K_cG_cQ_c & -5e_{xc}K_cS_c & 0 \\ 0 & 0 & 0 & 0 & 0 & 0 \\ \frac{7K_cS_c}{2} & 0 & -4e_{xc}K_cG_cS_c & -4e_{yc}K_cG_cS_c & 2K_cT_c & 0 \end{bmatrix} \tag{10}$$

$$\boldsymbol{B} = \frac{1}{n_c a_c}\begin{bmatrix} \frac{2e_c s_{f_c}}{\eta_c} & \frac{2(1+e_c c_{f_c})}{\eta_c} & 0 \\ -\frac{\eta_c e_c c_{f_c}}{1+\eta_c} - \frac{2\eta_c^2}{1+e_c c_{f_c}} & -\frac{\eta_c e_c[(2+e_c c_{f_c})s_{f_c}]}{(1+\eta_c)(1+e_c c_{f_c})} & 0 \\ \eta_c s_{\theta_c} & \eta_c \frac{(2+e_c c_{f_c})c_{\theta_c}+e_{xc}}{(1+e_c c_{f_c})} & \frac{\eta_c e_{yc} s_{\theta_c} Z_c}{(1+e_c c_{f_c})} \\ -\eta_c c_{\theta_c} & \eta_c \frac{(2+e_c c_{f_c})s_{\theta_c}+e_{yc}}{(1+e_c c_{f_c})} & -\frac{\eta_c e_{xc} s_{\theta_c} Z_c}{(1+e_c c_{f_c})} \\ 0 & 0 & \frac{\eta_c c_{\theta_c}}{(1+e_c c_{f_c})} \\ 0 & 0 & \frac{\eta_c s_{\theta_c}}{(1+e_c c_{f_c})} \end{bmatrix} \tag{11}$$

where f_c and $\theta_c = f_c + \omega_c$ are the mean true anomaly and true argument of latitude of the chief orbit respectively, and the following substitutions are applied for clarity

$$F_c = 4 + 3\eta_c\,,\ E_c = 1 + \eta_c\,,\ S_c = \sin(2i_c)\,,\ \Lambda_c = \frac{3}{2}n_c + \frac{7}{2}E_c K_c P_c T_c = \sin(i_c)^2\,,$$
$$Z_c = \mathrm{ctan}(i_c)\,,\ G_c = 1/\eta_c^2. \tag{12}$$

Due to the explicit dependence on the terms e_{xc} and e_{yc}, the plant matrix and the input matrix are time-varying and periodic. In fact, both e_{xc} and e_{yc} depend on the variation over time of the mean argument of perigee of the chief orbit, ω_c. Assuming that the chief is moving on a near-circular orbit (i.e. $e_c \to 0$), the matrices $\boldsymbol{A}$ and $\boldsymbol{B}$ can be further simplified neglecting the low-order terms, i.e., cancelling the terms proportional to e_c and e_c^2 as they are small compared to the others in Eqs. (10) and (11). In light of this, $\boldsymbol{A} = \boldsymbol{A}_{NC}$ and $\boldsymbol{B} = \boldsymbol{B}_{NC}$ being

$$\boldsymbol{A}_{NC} = \begin{bmatrix} 0 & 0 & 0 & 0 & 0 & 0 \\ -\Lambda_c & 0 & 0 & 0 & -K_c F_c S_c & 0 \\ 0 & 0 & 0 & -K_c Q_c & 0 & 0 \\ 0 & 0 & K_c Q_c & 0 & 0 & 0 \\ 0 & 0 & 0 & 0 & 0 & 0 \\ \frac{7K_c S_c}{2} & 0 & 0 & 0 & 2K_c T_c & 0 \end{bmatrix}, \boldsymbol{B}_{NC} = \frac{1}{n_c a_c}\begin{bmatrix} ccc0 & 2 & 0 \\ -2 & 0 & 0 \\ s_{u_c} & 2c_{u_c} & 0 \\ -c_{u_c} & 2s_{u_c} & 0 \\ 0 & 0 & c_{u_c} \\ 0 & 0 & s_{u_c} \end{bmatrix}. \tag{13}$$

In Eq. (13) $u_c = \omega_c + M_c$ indicates the mean argument of latitude of the chief orbit. Note that $u_c = u_c(t)$ and yields

$$u_c(t) = u_{c,0} + W_c(t - t_0), \tag{14}$$

where $W_c = n_c + K_c Q_c + \eta_c K_c P_c$. To simplify the notation the quantity $u_c(t)$ will be referred to as $u_{c,t}$ in the reminder.

2.4. Analytical solution for near-circular linear dynamics model

The solution of the linear system in Eq. (9), $\delta\boldsymbol{\alpha}(t)$, can be expressed as a function of the initial ROE state vector, $\delta\boldsymbol{\alpha}(t_0)$, and the forcing vector, $\boldsymbol{F}$, i.e.

$$\delta\boldsymbol{\alpha}(t) = \boldsymbol{\Phi}(t, t_0)\delta\boldsymbol{\alpha}(t_0) + \boldsymbol{\Psi}(t, t_0)\boldsymbol{F} \tag{15}$$

where $\boldsymbol{\Phi}(t,\ t_0)$ and $\boldsymbol{\Psi}(t,\ t_0)$ indicate the State Transition Matrix (STM) and the convolution matrix respectively. In [25] the authors derive the STM using the Floquet theory [31]. Hereafter the STM associated with near-circular linear relative dynamics model is reported for

completeness

$$\boldsymbol{\Phi}_{NC}(t,t_0)=\begin{bmatrix} 1 & 0 & 0 & 0 & 0 & 0\\ -\Lambda_c\Delta t & 1 & 0 & 0 & -K_cF_cS_c\Delta t & 0\\ 0 & 0 & c_{\Delta\omega} & -s_{\Delta\omega} & 0 & 0\\ 0 & 0 & s_{\Delta\omega} & c_{\Delta\omega} & 0 & 0\\ 0 & 0 & 0 & 0 & 1 & 0\\ \frac{7}{2}K_cS_c\Delta t & 0 & 0 & 0 & 2K_cT_c\Delta t & 1 \end{bmatrix} \tag{16}$$

where $\Delta t = t - t_0$ and $\Delta\omega = K_cQ_c\Delta t$. According to linear dynamics system theory [32], the corresponding convolution matrix, $\boldsymbol{\Psi}_{NC}(t, t_0)$, can be computed by solving the following integral,

$$\boldsymbol{\Psi}_{NC}(t,t_0)=\int_{t_0}^{t}\boldsymbol{\Phi}_{NC}(t,\tau)\boldsymbol{B}_{NC}(\boldsymbol{\alpha}_c(\tau))d\tau. \tag{17}$$

Substituting the STM and $\boldsymbol{B}_{NC}$ reported in Eqs. (16) and (13), respectively, into Eq. (17) yields

$$\boldsymbol{\Psi}_{NC}(t,t_0)=\frac{1}{a_cn_c}\int_{t_0}^{t}\begin{bmatrix} 0 & 2 & 0\\ -2 & -2\Lambda_c(t-\tau) & \bar{\psi}_1\\ \bar{\psi}_2 & 2\bar{\psi}_3 & 0\\ -\bar{\psi}_3 & 2\bar{\psi}_2 & 0\\ 0 & 0 & c_{(u_{c,0}+W_c(\tau-t_0))}\\ 0 & 7K_cS_c(t-\tau) & \bar{\psi}_4 \end{bmatrix}d\tau \tag{18}$$

where $u_{c,0}$ is the mean argument of latitude of the chief orbit at the instant t_0 and the terms $\bar{\psi}_i,\ i = 1, ..., 4$ are

$$\begin{aligned}\bar{\psi}_1 &= -F_cK_cS_cc_{(u_{c,0}+W_c(\tau-t_0))}(t-\tau)\bar{\psi}_2 = c_{K_cQ_c(t-\tau)}s_{(u_{c,0}+W_c(\tau-t_0))} + s_{K_cQ_c(t-\tau)}c_{(u_{c,0}+W_c(\tau-t_0))}\bar{\psi}_3\\ &= c_{K_cQ_c(t-\tau)}c_{(u_{c,0}+W_c(\tau-t_0))} - s_{K_cQ_c(t-\tau)}s_{(u_{c,0}+W_c(\tau-t_0))}\bar{\psi}_4 = s_{(u_{c,0}+W_c(\tau-t_0))}\\ &\quad + 2K_cT_cc_{(u_{c,0}+W_c(\tau-t_0))}(t-\tau).\end{aligned} \tag{19}$$

According with Eqs. (18) and (19), the convolution matrix $\boldsymbol{\Psi}_{NC}(t, t_0)$ becomes

$$\boldsymbol{\Psi}_{NC}(t,t_0)=\frac{1}{a_cn_cW_c}\begin{bmatrix} 0 & 2\Delta u & 0\\ -2\Delta u & -\frac{\Lambda_c\Delta u^2}{W_c} & \psi_1\\ \psi_2 & 2\psi_3 & 0\\ -\psi_3 & 2\psi_2 & 0\\ 0 & 0 & (s_{u_{c,t}}-s_{u_{c,0}})\\ 0 & \frac{7}{2}\frac{K_cS_c\Delta u^2}{W_c} & \psi_4 \end{bmatrix} \tag{20}$$

being $\Delta u = u_{c,t} - u_{c,0}$. In Eq. (20) the terms $\psi_i,\ i = 1, ..., 4,$ are

$$\begin{aligned}\psi_1 &= W_c\int_{t_0}^{t}\bar{\psi}_1d\tau = \frac{F_cK_cS_c}{W_c}\left(c_{u_{c,t}}-c_{u_{c,0}}+s_{u_{c,0}}\Delta u\right)\psi_2 = W_c\int_{t_0}^{t}\bar{\psi}_2d\tau = -\frac{1}{\beta}\left(c_{u_{c,t}}-c_{(u_{c,0}+C\Delta u)}\right)\psi_3\\ &= W_c\int_{t_0}^{t}\bar{\psi}_3d\tau = \frac{1}{\beta}\left(s_{u_{c,t}}-s_{(u_{c,0}+C\Delta u)}\right)\psi_4 = W_c\int_{t_0}^{t}\bar{\psi}_4d\tau\\ &= -\frac{1}{W_c}\left((W_c+2K_cT_c)(c_{u_{c,t}}-c_{u_{c,0}})+2K_cT_cs_{u_{c,0}}\Delta u\right)\end{aligned} \tag{21}$$

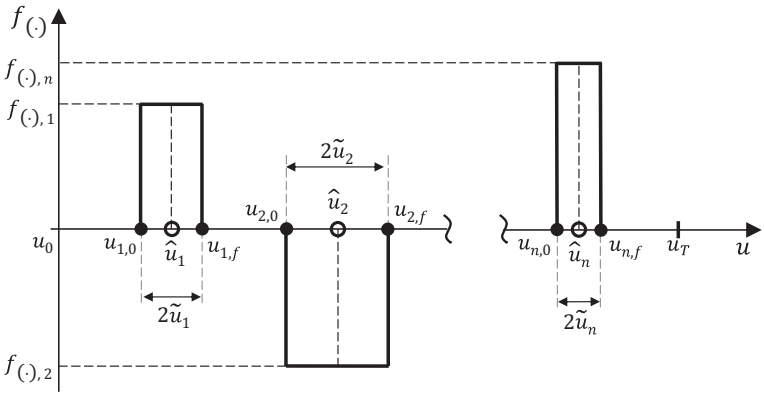

Fig. 1. Example of continuous on/off control profile.

whereas β and C are constant coefficients that depend on mean semi-major axis, eccentricity, and inclination of the chief orbit as follows

$$C = \frac{K_c Q_c}{W_c}, \quad \beta = 1 - C. \tag{22}$$

3. Reconfiguration control problem

This section reports the piecewise continuous and impulsive control solutions derived for the in-plane and out-of-plane spacecraft formation reconfiguration, pointing out the similarities and the differences between the aforementioned formulations. First, the general methodology used to obtain both impulsive and continuous solutions is presented. It consists of the following steps: (1) the expression of the final mean ROE state, $\delta\boldsymbol{\alpha}(T)$, is derived, (2) then, given a desired mean relative orbit, $\delta\boldsymbol{\alpha}_{des}$, the expression $\delta\boldsymbol{\alpha}(T) = \delta\boldsymbol{\alpha}_{des}$ is solved for the parameters that describe the control profile, i.e. the maneuvers' locations and amplitudes. In further details, 2- and 3-maneuver strategies are investigated for in-plane relative motion control, whereas a single cross-track maneuver is considered for the out-of-plane formation reconfiguration. As discussed in the following sections, the boundary condition $\delta\boldsymbol{\alpha}(T) = \delta\boldsymbol{\alpha}_{des}$ cannot be always solved analytically, therefore, some of the presented control strategies involve an iterative numerical algorithm to determine the control acceleration profile.

3.1. Mathematical formulation

Let us consider n extended maneuvers of magnitude $\boldsymbol{F}_j = [f_{x,j}, f_{y,j}, f_{z,j}]^T$ and duration Δt_j, with $j = 1, \dots, n$, as illustrated in Fig. 1 for a generic axis $(\cdot)$. Using the near-circular linearized model discussed in the previous section, the relative state at the end of each j-th maneuver $\delta\boldsymbol{\alpha}(t_{j,f})$ can be expressed as a function of $\delta\boldsymbol{\alpha}(t_{j,0})$, the maneuver durations Δt_j, and thrust magnitudes as follows (see Eq. (15)),

$$\delta\boldsymbol{\alpha}_{j,f} = \delta\boldsymbol{\alpha}(t_{j,f}) = \boldsymbol{\Phi}(t_{j,f}, t_{j,0})\delta\boldsymbol{\alpha}(t_{j,0}) + \boldsymbol{\Psi}(t_{j,f}, t_{j,0})\boldsymbol{F}_j, \quad j = 1, ..., n \tag{23}$$

where $t_{j,0}$ and $t_{j,f}$ indicate the initial and the final instants of the j-th maneuver respectively. Note that the instant $t_{j,f}$ can be expressed as a function of the firing duration Δt_j as

$t_{j,f} = t_{j,0} + \Delta t_j$. According to Eq. (23), the mean ROE at the end of maneuvering interval, $\delta\boldsymbol{\alpha}(T)$, depends on the mean ROE at the initial maneuver time $\delta\boldsymbol{\alpha}(t_0)$, the n maneuver durations, Δt_j, and the thrust vector, $\boldsymbol{F}_j$,

$$\begin{aligned}
\delta\boldsymbol{\alpha}_{1,0} &= \delta\boldsymbol{\alpha}(t_{1,0}) = \boldsymbol{\Phi}_{NC}(t_{1,0}, t_0)\delta\boldsymbol{\alpha}(t_0) = \boldsymbol{\Phi}_{NC}(t_{1,0}, t_0)\delta\boldsymbol{\alpha}_0 \\
\delta\boldsymbol{\alpha}_{1,f} &= \boldsymbol{\Phi}_{NC}(t_{1,f}, t_{1,0})\delta\boldsymbol{\alpha}_{1,0} + \boldsymbol{\Psi}_{NC}(t_{1,f}, t_{1,0})\boldsymbol{F}_1 \\
&= \boldsymbol{\Phi}_{NC}(t_{1,f}, t_0)\delta\boldsymbol{\alpha}_0 + \boldsymbol{\Psi}_{NC}(t_{1,f}, t_{1,0})\boldsymbol{F}_1 \\
\delta\boldsymbol{\alpha}_{2,0} &= \boldsymbol{\Phi}_{NC}(t_{2,0}, t_{1,f})\delta\boldsymbol{\alpha}_{1,f} = \boldsymbol{\Phi}_{NC}(t_{2,0}, t_0)\delta\boldsymbol{\alpha}_0 \\
&\quad + \boldsymbol{\Phi}_{NC}(t_{2,0}, t_{1,f})\boldsymbol{\Psi}_{NC}(t_{1,f}, t_{1,0})\boldsymbol{F}_1 \\
\delta\boldsymbol{\alpha}_{2,f} &= \boldsymbol{\Phi}_{NC}(t_{2,f}, t_{2,0})\delta\boldsymbol{\alpha}_{2,0} + \boldsymbol{\Psi}_{NC}(t_{2,f}, t_{2,0})\boldsymbol{F}_2 \\
&= \boldsymbol{\Phi}_{NC}(t_{2,f}, t_0)\delta\boldsymbol{\alpha}_0 + \boldsymbol{\Phi}_{NC}(t_{2,f}, t_{1,f})\boldsymbol{\Psi}_{NC}(t_{1,f}, t_{1,0})\boldsymbol{F}_1 \\
&\quad + \boldsymbol{\Psi}_{NC}(t_{2,f}, t_{2,0})\boldsymbol{F}_2 \\
\delta\boldsymbol{\alpha}_T &= \boldsymbol{\Phi}_{NC}(T, t_0)\delta\boldsymbol{\alpha}_0 + \sum_{j=1}^{n} \boldsymbol{\Phi}_{NC}(T, t_{j,f})\boldsymbol{\Psi}_{NC}(t_{j,f}, t_{j,0})\boldsymbol{F}_j
\end{aligned} \tag{24}$$

Note that Eq. (24) is valid if $t_{j,0} \geq t_{j-1,f}$. If $\delta\boldsymbol{\alpha}_0$ is fixed and Δt_j is considered an user-defined parameter, the reconfiguration problem is to find the thrust magnitudes, $\boldsymbol{F}_j$, and their application times, $t_{j,0}$ (or alternatively the maneuver mid-point instant, i.e. $t_j = (t_{j,0} + t_{j,f})/2$), that satisfy the following equation

$$\begin{aligned}
\Delta\delta\boldsymbol{\alpha}_{des} &= \delta\boldsymbol{\alpha}_{des} - \boldsymbol{\Phi}_{NC}(T, t_0)\delta\boldsymbol{\alpha}_0 \\
&= \sum_{j=1}^{n} \boldsymbol{\Phi}_{NC}(T, t_{j,f})\boldsymbol{\Psi}_{NC}(t_{j,f}, t_{j,0})\boldsymbol{F}_j.
\end{aligned} \tag{25}$$

The term $\delta\boldsymbol{\alpha}_{des}$ is the desired mean ROE vector at the end of the maneuvering interval. Eq. (25) represents a set of 6 nonlinear equations in (3+1)n unknowns (i.e., $\boldsymbol{F}_j$ and t_j with $j = 1, ..., n$). Note that the maneuver duration Δt_j is assumed to be known. Accordingly, at least two maneuvers are needed to obtain a finite number of solutions. The control thrust profile is a function of $\delta\boldsymbol{\alpha}_0$, the maneuver durations, Δt_j, and desired ROE state, $\delta\boldsymbol{\alpha}_{des}$. It is noteworthy that when a sequence of n impulsive maneuvers is considered to accomplish the formation reconfiguration, the approach described by Eq. (24) leads to, [5]

$$\begin{aligned}
\Delta\delta\boldsymbol{\alpha}_{des} &= \delta\boldsymbol{\alpha}_{des} - \boldsymbol{\Phi}_{NC}(T, t_0)\delta\boldsymbol{\alpha}_0 \\
&= \sum_{j=1}^{n} \boldsymbol{\Phi}_{NC}(T, t_j)\boldsymbol{B}_{NC}(u_{c,j})\Delta\boldsymbol{v}_j.
\end{aligned} \tag{26}$$

where $\Delta\boldsymbol{v}_j = [\Delta v_{x,j}, \Delta v_{y,j}, \Delta v_{z,j}]^T$ denotes the impulses vector whereas $u_{c,j}$ is the mean argument of latitude at the maneuver time, t_j. In [5] the authors derived the analytical control solutions in near-circular perturbed orbits using three along-track impulses and one cross-track impulse for in-plane and out-of-plane reconfigurations respectively, whereas in [23] the authors of this paper derived the corresponding analytical piecewise continuous solutions. This paper aims at extending the aforementioned previous works by determining the 2- and 3-maneuver continuous and impulsive solutions for in-plane reconfiguration control. Moreover, this work will present a comparison between the proposed control strategies, identifying the related pros and cons.

3.2. In-plane reconfiguration

In this section the in-plane reconfiguration problem is addressed, i.e. only the relative mean semi-major axis, the relative mean longitude, and the relative eccentricity vector are assumed to be controlled over the maneuvering interval. Note that the in-plane reconfiguration problem involves the solution of 4 nonlinear equations (i.e., the first four rows of Eq. (25) or Eq. (26) for piecewise continuous and impulsive strategies respectively) in $(2+1)n$ unknowns (i.e., $2n$ in-plane components of thrust or impulses vectors and n maneuvers' locations). If a sequence of in-plane finite-time maneuvers, $\boldsymbol{F}_j = [f_{x,j}, f_{y,j}, 0]^T$ with $j = 1, ..., n$, is considered, Eq. (25) becomes

$$\sum_{j=1}^{n} \tilde{u}_j f_{y,j} = \frac{\mu}{\beta} \Delta\delta a_{des} \tag{27a}$$

$$\sum_{j=1}^{n} \left[\tilde{u}_j \left(\frac{\Lambda_c}{W_c} \left(u_T - \hat{u}_j \right) f_{y,j} + f_{x,j} \right) \right] = -\frac{\mu}{\beta} \Delta\delta\lambda_{des} \tag{27b}$$

$$\sum_{j=1}^{n} \left[\sin\left(\beta\tilde{u}_j\right) \left(\cos\left(Cu_T + \beta\hat{u}_j\right) f_{y,j} + \sin\left(Cu_T + \beta\hat{u}_j\right) \frac{f_{x,j}}{2} \right) \right] = \mu \Delta\delta e_{x,des} \tag{27c}$$

$$\sum_{j=1}^{n} \left[\sin\left(\beta\tilde{u}_j\right) \left(\sin\left(Cu_T + \beta\hat{u}_j\right) f_{y,j} - \cos\left(Cu_T + \beta\hat{u}_j\right) \frac{f_{x,j}}{2} \right) \right] = \mu \Delta\delta e_{y,des} \tag{27d}$$

where

$$\mu = \beta \frac{W_c n_c a_c}{4} \tag{28}$$

and

$$\hat{u}_j = \frac{u_{j,f} + u_{j,0}}{2}, \quad \tilde{u}_j = \frac{u_{j,f} - u_{j,0}}{2}, \quad j = 1, ..., 3 \tag{29}$$

being $u_{j,0}$ and $u_{j,f}$ the mean argument of latitude of the chief orbit at the instants $t_{j,0}$ and $t_{j,f}$, respectively. Accordingly, $\hat{u}_{j,y}$ is the mid-point maneuver location and $\tilde{u}_{j,y}$ is half the duration of the j-th maneuver. It is worth remarking that the extended maneuvers along x and y axes of the RTN reference are assumed to last the same interval of time. Eq. (27) can be simplifed by defining the following variables,

$$\begin{aligned} U_{j,0} &= \beta u_{j,0} + Cu_T, \qquad U_{j,f} = \beta u_{j,f} + Cu_T, \\ \widetilde{U}_j &= \frac{U_{j,f} - U_{j,0}}{2} = \beta\tilde{u}_j, \qquad \widehat{U}_j = \frac{U_{j,f} + U_{j,0}}{2} = Cu_T + \beta\hat{u}_j. \end{aligned} \tag{30}$$

The term U can be seen as a *perturbed* mean argument of latitude due to the J_2. Hence, $\widetilde{U}_j$ is related to half the duration of the j-th maneuver and $\widehat{U}_j$ is related to the mid-point maneuver location. Substituting Eq. (30) in Eq. (27) yields,

$$\sum_{j=1}^{n} \widetilde{U}_j f_{y,j} = \mu \Delta\delta a_{des} \tag{31a}$$

$$\sum_{j=1}^{n}\left[\widetilde{U}_j\left(\frac{\Lambda_c}{\beta W_c}\left(u_T-\widehat{U}_j\right)f_{y,j}+f_{x,j}\right)\right]=-\mu\Delta\delta\lambda_{des} \tag{31b}$$

$$\sum_{j=1}^{n}\left[\sin\widetilde{U}_j\left(\cos\widehat{U}_j f_{y,j}+\frac{1}{2}\sin\widehat{U}_j f_{x,j}\right)\right]=\mu\Delta\delta e_{x,des} \tag{31c}$$

$$\sum_{j=1}^{n}\left[\sin\widetilde{U}_j\left(\sin\widehat{U}_j f_{y,j}-\frac{1}{2}\cos\widehat{U}_j f_{x,j}\right)\right]=\mu\Delta\delta e_{y,des} \tag{31d}$$

Similarly, the equations governing the variation of the mean ROE due to a sequence of impulsive maneuvers are (see Eq. 26)

$$2\sum_{j=1}^{n}\Delta v_{y,j}=n_c a_c\Delta\delta a_{des} \tag{32a}$$

$$2\sum_{j=1}^{n}\left(\frac{\Lambda_c}{W_c\beta}\left(u_T-\widehat{U}_j\right)\Delta v_{y,j}+\Delta v_{x,j}\right)=-n_c a_c\Delta\delta\lambda_{des} \tag{32b}$$

$$\sum_{j=1}^{n}\left(2\cos\widehat{U}_j\Delta v_{y,j}+\sin\widehat{U}_j\Delta v_{x,j}\right)=n_c a_c\Delta\delta e_{x,des} \tag{32c}$$

$$\sum_{j=1}^{n}\left(2\sin\widehat{U}_j\Delta v_{y,j}-\cos\widehat{U}_j\Delta v_{x,j}\right)=n_c a_c\Delta\delta e_{y,des} \tag{32d}$$

It is worth pointing out that Eq. (31) converges to Eq. (32) when $\widetilde{U}_j\to 0$. This is straightforward by recognizing that

$$\Delta v_{(\cdot)}=2\frac{\tilde{u}f_{(\cdot)}}{W_c}=2\frac{\widetilde{U}f_{(\cdot)}}{\beta W_c} \tag{33}$$

and $\sin\widetilde{U}_j\approx\widetilde{U}_j$ when $\widetilde{U}_j\to 0$. This means that even the piecewise continuous in-plane solutions will tend to the corresponding impulsive ones for $\widetilde{U}_j\to 0$.

The following sections present the mathematical expressions of in-plane control solutions given by 2- and 3-maneuver schemes, considering different combinations of tangential (T) and radial (R) maneuvers. Note that the 2-maneuver solutions accomplish the final in-plane formation reconfiguration through the minimum number of maneuvers. However, as discussed in Section 3.2.2, when only radial maneuvers are performed only three ROEs can be established. In addition, the 3-maneuver scheme through tangential impulses leads to the minimum delta-v solution for the corresponding fuel-optimal impulsive reconfiguration problem, as discussed by Chernick et al. in [5].

3.2.1. T-T-T maneuver

Let us consider that only three tangential impulses are performed by the deputy spacecraft, i.e.,

$$\boldsymbol{\Delta} v_j^T = [0, \Delta v_{y,j}, 0]^T \quad with \quad j = 1, ..., 3. \tag{34}$$

As discussed by Chernick et al. in [5], this choice allows one to find a minimum delta-V solution when the reconfiguration cost is driven by the variation of relative eccentricity vector (i.e., $\Delta\delta e_{des} > \Delta\delta a_{des}$ and $\Delta\delta e_{des} > 2\Delta\delta\lambda_{des}/3\Delta u$ with $\Delta\delta e_{des} = \sqrt{\Delta\delta e_{x,des}^2 + \Delta\delta e_{y,des}^2}$ and $\Delta u = (u_T - u_0)$). The solution of Eq. (27) for the impulses' locations, U_j, and magnitudes, $\Delta v_{y,j}$, is given by

$$U_1 = \overline{U}_y + k_1\pi\,, \quad U_2 = U_1 + k_2\pi\,, \quad U_3 = U_1 + k_3\pi \tag{35}$$

$$\Delta v_{y,j} = -\frac{a_c n_c \xi_j}{2\pi\Lambda_c\left(k_2\left(1-(-1)^{k_3}\right) - k_3\left(1-(-1)^{k_2}\right)\right)}\,, \quad j = 1, 2, 3 \tag{36}$$

where the following quantities have been introduced for clarity

$$\overline{U}_y = \tan^{-1}\left(\frac{\Delta\delta e_{y,des}}{\Delta\delta e_{x,des}}\right) \tag{37}$$

$$\xi_1 = (-1)^{k_2}\varphi_1 - (-1)^{k_3}\varphi_2 + (-1)^{k_1}\pi\Lambda_c\Delta\delta e_{des}(k_3 - k_2) \tag{38a}$$

$$\xi_2 = \varphi_1 - (-1)^{k_3}\varphi_3 + (-1)^{k_1}k_3\pi\Lambda_c\Delta\delta e_{des} \tag{38b}$$

$$\xi_3 = \varphi_2 - (-1)^{k_2}\varphi_3 + (-1)^{k_1}k_2\pi\Lambda_c\Delta\delta e_{des} \tag{38c}$$

$$\varphi_j = (u_T - U_j)\Lambda_c\Delta\delta a_{des} + \beta W_c\Delta\delta\lambda_{des}\,, \quad j = 1, 2, 3 \tag{39}$$

Note that the above solution coincides with that one derived in [5]. However a different representation is used here to point out the similarity with the continuous formulation. Eq. (36) becomes singular when $k_2 = 2\,n_2$ and $k_3 = 2\,n_3$, with $n_2,\ n_3 \in \mathbb{N}$.

The piecewise continuous solution is obtained by solving the system of nonlinear equations (31), assuming that $f_{x,j} = 0$ with $j = 1, .., 3$. One solution family among the possible infinite solutions is given by

$$\widehat{U}_1 = \overline{U}_y + k_1\pi\,, \quad \widehat{U}_2 = \widehat{U}_1 + k_2\pi, \quad \widehat{U}_3 = \widehat{U}_1 + k_3\pi \tag{40}$$

$$f_{y,j} = -\frac{\mu}{D}\Xi_j\,, \quad j = 1, 2, 3, \tag{41}$$

where $k_1, k_2 \in \mathbb{N}$ and the quantities D and Ξ_j are defined as follows

$$D = \pi \Lambda_c \Big(k_2 \widetilde{U}_2 \Big(\widetilde{U}_3 \sin \widetilde{U}_1 - (-1)^{k_3} \widetilde{U}_1 \sin \widetilde{U}_3 \Big) - k_3 \widetilde{U}_3 \Big(\widetilde{U}_2 \sin \widetilde{U}_1 - (-1)^{k_2} \widetilde{U}_1 \sin \widetilde{U}_2 \Big) \Big) \tag{42}$$

$$\Xi_1 = (-1)^{k_2} \widetilde{U}_3 \sin \widetilde{U}_2 \Phi_1 - (-1)^{k_3} \widetilde{U}_2 \sin \widetilde{U}_3 \Phi_2 + (-1)^{k_1} \widetilde{U}_2 \widetilde{U}_3 \pi \Lambda_c \Delta\delta e_{des} (k_3 - k_2) \tag{43a}$$

$$\Xi_2 = \widetilde{U}_3 \sin \widetilde{U}_1 \Phi_1 - (-1)^{k_3} \widetilde{U}_1 \sin \widetilde{U}_3 \Phi_3 + (-1)^{k_1} \widetilde{U}_1 \widetilde{U}_3 k_3 \pi \Lambda_c \Delta\delta e_{des} \tag{43b}$$

$$\Xi_3 = \widetilde{U}_2 \sin \widetilde{U}_1 \Phi_2 - (-1)^{k_2} \widetilde{U}_1 \sin \widetilde{U}_2 \Phi_3 + (-1)^{k_1} \widetilde{U}_1 \widetilde{U}_2 k_2 \pi \Lambda_c \Delta\delta e_{des} \tag{43c}$$

$$\Phi_j = (u_T - \widehat{U}_j) \Lambda_c \Delta\delta a_{des} + \beta W_c \Delta\delta \lambda_{des}\,, \quad j = 1, 2, 3 \tag{44}$$

Ξ_j, and Φ_j represent the continuous counterpart of the impulsive quantities ξ_j, and φ_j. It is noteworthy that in this case when $k_2 = 2\,n_2$ and $k_3 = 2\,n_3$, with $n_2,\ n_3 \in \mathbb{N}$, the denominator in Eq. (41), D, does not go to zero if $\widetilde{U}_1 \neq \widetilde{U}_2 \neq \widetilde{U}_3$. Differently form the impulsive solution, the piecewise one exists even when the quantities k_2 and k_3 are even.

The solution given by Eqs. (40) and (41) can be modified to include the thrust level constraint that might arise from the operational limitations of onboard thrusters. For the sake of the example, let us assume that the maneuverable satellite is equipped with thrusters capable of operating only in on/off configurations with a specific acceleration magnitude, f_{max}. The problem is to update the maneuvers' durations, $\widetilde{U}_j$, such that the control profile has the user-defined magnitude f_{max}. In order to find the updated values $\widetilde{U}_j^{up}$ with $j = 1, ..., 3$, Eqs. (31a-d) (with $f_{x,j} = 0$ and $f_{y,j}^{up} = sgn(f_{y,j}) f_{max}$) have to be solved for $\widetilde{U}_j^{up}$. Since Eqs. (31a-b) are linear in the unknows $\widetilde{U}_j^{up}$, the expressions of $\widetilde{U}_1^{up}$ and $\widetilde{U}_2^{up}$ can be found as function of $\widetilde{U}_3^{up}$. Being $f_{y,j}^{up} = sgn(f_{y,j}) f_{max}$, $\widetilde{U}_1^{up}$ and $\widetilde{U}_2^{up}$ can be computed as follows

$$\widetilde{U}_1^{up} = \frac{4\Lambda_c \widetilde{U}_3^{up} f_{y,3}^{up} \big(\widehat{U}_2 - \widehat{U}_3\big) + \beta^2 W_c H_c \Delta\delta\lambda_{des} - \Lambda_c H_c \Delta\delta a_{des} \big(u_T - \beta \widehat{U}_2\big)}{(4\Lambda_c f_{y,1}^{up} (\widehat{U}_1 - \widehat{U}_2))} \tag{45}$$

$$\widetilde{U}_2^{up} = -\frac{4\Lambda_c \widetilde{U}_3^{up} f_{y,3}^{up} \big(\widehat{U}_1 - \widehat{U}_3\big) + \beta^2 W_c H_c \Delta\delta\lambda_{des} - \Lambda_c H_c \Delta\delta a_{des} \big(u_T - \beta \widehat{U}_1\big)}{(4\Lambda_c f_{y,2}^{up} (\widehat{U}_1 - \widehat{U}_2))} \tag{46}$$

with

$$H_c = W_c a_c n_c. \tag{47}$$

Substituting Eqs. (45) and (46) into Eq. (31d) gives the following nonlinear equation in the unknown $\widetilde{U}_3^{up}$,

$$f_{y,3}^{up} \sin \widehat{U}_3 \sin \widetilde{U}_3^{up} + f_{y,1}^{up} \sin \widehat{U}_1 \sin \rho_1 - f_{y,2}^{up} \sin \widehat{U}_2 \sin \rho_2 = \mu \Delta\delta e_{y,des} \tag{48}$$

where

$$\begin{aligned}\rho_1 &= \frac{4\Lambda_c \widetilde{U}_3^{up} f_{y,3}^{up}(\widehat{U}_2-\widehat{U}_3)+\beta^2 W_c H_c \Delta\delta\lambda_{des}-\Lambda_c H_c \Delta\delta a_{des}\left(u_T-\beta\widehat{U}_2\right)}{(4\Lambda_c f_{y,1}^{up}(\widehat{U}_1-\widehat{U}_2))}\\ \rho_2 &= \frac{4\Lambda_c \widetilde{U}_3^{up} f_{y,3}^{up}(\widehat{U}_1-\widehat{U}_3)+\beta^2 W_c H_c \Delta\delta\lambda_{des}-\Lambda_c H_c \Delta\delta a_{des}\left(u_T-\beta\widehat{U}_1\right)}{(4\Lambda_c f_{y,2}^{up}(\widehat{U}_1-\widehat{U}_2))}\end{aligned} \tag{49}$$

and the quantity μ is given by Eq. (28). An iterative algorithm can be used to solve Eq. (48). An initial guess that guarantees a fast convergence of the algorithm can be chosen by analyzing the error function J,

$$J = f_{y,3}^{up}\sin\widehat{U}_3\sin\widetilde{U}_3^{up} + f_{y,1}^{up}\sin\widehat{U}_1\sin\rho_1 - f_{y,2}^{up}\sin\widehat{U}_2\sin\rho_2 - \mu\Delta\delta e_{y,des}, \tag{50}$$

Note that the quantity $\widetilde{U}_3^{up}$ has to be such that the control profile is included in the interval $[u_0,\ u_T]$, i.e. the following inequalities have to be satisfied,

$$\widetilde{U}_1^{up} < \widehat{U}_1 - cu_T \tag{51a}$$

$$\widetilde{U}_3^{up} < u_T - \widehat{U}_3 \tag{51b}$$

$$\widetilde{U}_1^{up} + \widetilde{U}_2^{up} < \widehat{U}_2 - \widehat{U}_1 \tag{51c}$$

$$\widetilde{U}_2^{up} + \widetilde{U}_3^{up} < \widehat{U}_3 - \widehat{U}_2. \tag{51d}$$

Finally, the method described above for the correction of the analytical solution can be summarized as follows:

1. set the value of available control acceleration, f_{max};
2. compute the error function $J(\widetilde{U}_3^{up})$ from Eq. (50) with $\widetilde{U}_3^{up} \in (0, u_T)$;
3. evaluate Eq. (51) to find the feasible values of maneuver duration, $\widetilde{U}_{3,feas.}^{up} \subset \widetilde{U}_3^{up}$;
4. evaluate the sign of $J(\widetilde{U}_{3,feas.}^{up})$ at the boundaries of the domain, $a = min(\widetilde{U}_{3,feas.}^{up})$ and $b = max(\widetilde{U}_{3,feas.}^{up})$;
5. if $sgn(J(a)) \neq sgn(J(b))$, find $\widetilde{U}_{3,ig}^{up}$ that minimizes $|J(\widetilde{U}_{3,feas.}^{up})|$ and run the *fzero* routine to compute the root of $J(\widetilde{U}_{3,feas.}^{up})$, otherwise go to step 1 and change the value of f_{max} (if it is compatible with the actuator capability).

3.2.2. R-R maneuver

The entire ROE state cannot be controlled using two radial maneuvers, thus the in-plane reconfiguration problem as defined in Section 3.2 does not admit solutions. In fact, the relative drift can be changed only using tangential maneuvers. However, a couple of pure radial maneuvers still enables the adjustment of $\Delta\delta\lambda$, $\Delta\delta e_x$ and $\Delta\delta e_y$. Hence, solving Eq. (32) (with $\Delta v_{y,j} = 0$) for the maneuvers locations, U_j, and velocity changes, $\Delta v_{x,j}$, leads to the following expressions

$$U_1 = \overline{U}_x + k_1\pi\ ,\ U_2 = U_1 + k_2\pi, \tag{52}$$

$$\Delta v_{x,1} = \frac{a_c n_c\left((-1)^{k_2}\Delta\delta\lambda_{des} - 2(-1)^{k_1}\Delta\delta e_{des}\right)}{2\left(1-(-1)^{k_2}\right)}, \tag{53}$$

$$\Delta v_{x,2} = \frac{a_c n_c \left(-\Delta\delta\lambda_{des} + 2\,(-1)^{k_1}\Delta\delta e_{des}\right)}{2\left(1-(-1)^{k_2}\right)}. \tag{54}$$

where $k_1, k_2 \in \mathbb{N}$ and

$$\overline{U}_x = -\tan^{-1}\left(\frac{\Delta\delta e_{x,des}}{\Delta\delta e_{y,des}}\right). \tag{55}$$

The continuous solution can be obtained by considering the same maneuvers' separation, i.e.,

$$\widehat{U}_1 = \overline{U}_x + k_1\pi\ ,\ \widehat{U}_2 = \widehat{U}_1 + k_2\pi, \tag{56}$$

and solving the Eq. (31) (with $f_{y,j} = 0$). Then, the thrust amplitudes are given by the following expressions

$$f_{x,1} = \mu\frac{(-1)^{k_2}\Delta\delta\lambda_{des}\sin\widetilde{U}_2 - 2(-1)^{k_1}\Delta\delta e_{des}\widetilde{U}_2}{\widetilde{U}_2\sin\widetilde{U}_1 - (-1)^{k_2}\widetilde{U}_1\sin\widetilde{U}_2}, \tag{57}$$

$$f_{x,2} = \mu\frac{-\Delta\delta\lambda_{des}\sin\widetilde{U}_1 + 2(-1)^{k_1}\Delta\delta e_{des}\widetilde{U}_1}{\widetilde{U}_2\sin\widetilde{U}_1 - (-1)^{k_2}\widetilde{U}_1\sin\widetilde{U}_2}. \tag{58}$$

As for the T-T-T maneuver combination, also in this case the continuous solution extends the domain of the solution. In fact, comparing Eqs. (53) and (54) with Eqs. (57) and (58), when $k_2 = 2n_2\pi$ with $n_2 \in \mathbb{N}$, the impulsive solution is singular, whereas the continuous one still exists if $\widetilde{U}_1 \neq \widetilde{U}_2$.

It is noteworthy that the maneuver cost for the impulsive and the piecewise continuous schemes are the same. In fact, it can be proven that $\Delta v_{1,x} + \Delta v_{2,x} = 2(\widetilde{U}_1 f_{x,1} + \widetilde{U}_2 f_{x,2})/(\beta W_c)$. The above statement is valid only for the R-R scheme and is assessed by numerical simulations reported in Section 4.

3.2.3. RT-RT maneuver

Here, a couple of radial/tangential maneuvers is considered to control the relative configuration of the formation. According with the approach proposed in this paper, a solution of Eq. (32) can be determined imposing a separation between the impulses of $k_2\pi$, i.e.

$$U_1 = \overline{U}_y + k_1\pi\ ,\ U_2 = U_1 + k_2\pi, \tag{59}$$

with $k_1, k_2 \in \mathbb{N}$ and $\overline{U}_y$ defined by Eq. (40). The four impulses are computed by the following formulas,

$$\Delta v_{x,1} = \frac{a_c n_c\Big(-\varphi_1 + (-1)^{k_2}\varphi_2 + (-1)^{k_1}(-1)^{k_2}k_2\pi\,\Lambda_c\Delta\delta e_{des}\Big)}{4\beta W_c\Big(1-(-1)^{k_2}\Big)} \tag{60}$$

$$\Delta v_{x,2} = \frac{a_c n_c\Big((-1)^{k_2}\varphi_1 - \varphi_2 - (-1)^{k_1}k_2\pi\,\Lambda_c\Delta\delta e_{des}\Big)}{4\beta W_c\Big(1-(-1)^{k_2}\Big)} \tag{61}$$

$$\Delta v_{y,1} = \frac{a_c n_c}{4}\left(\Delta\delta a_{des} + (-1)^{k_1}\Delta\delta e_{des}\right) \tag{62}$$

$$\Delta v_{y,2} = \frac{a_c n_c}{4}\left(\Delta\delta a_{des} - (-1)^{k_1}\,\Delta\delta e_{des}\right), \tag{63}$$

In light of the above, the impulsive solution exists only if $k_2 \neq 2n_2$, $n_2 \in \mathbb{N}$. If the exponents k_2 and k_3 in Eqs. (60) and (61) are odd, the quantities $\Delta v_{x,1}$ and $\Delta v_{x,2}$ are equal in magnitude and direction, i.e., $\Delta v_{x,1} - \Delta v_{x,2} = 0$. In addition, when $\Delta a_{des} = 0$, the sum of the tangential components must be equal to zero to meet the constraints on the final formation configuration, i.e., $\Delta v_{y,1} + \Delta v_{y,2} = 0$.

Given the similarity between the impulsive and continuous formulations, a class of solutions among the infinite available ones for the Eq. (31) can be derived as follows,

$$\widehat{U}_1 = \overline{U}_y + k_1\pi\ ,\ \widehat{U}_2 = \widehat{U}_1 + k_2\pi \tag{64}$$

$$f_{x,1} = \frac{a_c n_c \sin\widetilde{U}_2\,\Xi_1}{4\left(\widetilde{U}_1\sin\widetilde{U}_2 - (-1)^{k_2}\widetilde{U}_2\sin\widetilde{U}_1\right)^2} \tag{65}$$

$$f_{x,2} = \frac{a_c n_c \sin\widetilde{U}_1\,\Xi_2}{4\left(\widetilde{U}_1\sin\widetilde{U}_2 - (-1)^{k_2}\widetilde{U}_2\sin\widetilde{U}_1\right)^2} \tag{66}$$

$$f_{y,1} = \frac{\mu\left(\sin\widetilde{U}_2\Delta\delta a_{des} - (-1)^{k_1}(-1)^{k_2}\widetilde{U}_2\Delta\delta e_{des}\right)}{\widetilde{U}_1\sin\widetilde{U}_2 - (-1)^{k_2}\widetilde{U}_2\sin\widetilde{U}_1} \tag{67}$$

$$f_{y,2} = \frac{-\mu(-1)^{k_2}\left(\sin\widetilde{U}_1\Delta\delta a_{des} - (-1)^{k_1}\widetilde{U}_1\Delta\delta e_{des}\right)}{\widetilde{U}_1\sin\widetilde{U}_2 - (-1)^{k_2}\widetilde{U}_2\sin\widetilde{U}_1} \tag{68}$$

where

$$\begin{aligned}\Xi_1 =& -\widetilde{U}_1\sin\widetilde{U}_2\Phi_1 + (-1)^{k_2}\widetilde{U}_2\sin\widetilde{U}_1\Phi_2 \\ &+ (-1)^{k_1}(-1)^{k_2}\widetilde{U}_1\widetilde{U}_2 k_2\pi\,\Lambda_c\Delta\delta e_{des}\end{aligned} \tag{69}$$

$$\Xi_2 = (-1)^{k_2}\widetilde{U}_1\sin\widetilde{U}_2\Phi_1 - \widetilde{U}_2\sin\widetilde{U}_1\Phi_2 - (-1)^{k_1}\widetilde{U}_1\widetilde{U}_2 k_2\pi\,\Lambda_c\Delta\delta e_{des}. \tag{70}$$

From Eqs. (65)–(68), it is clear that the solution exists only if $k_2 \neq 2n_2$, with $n_2 \in \mathbb{N}$, or $\widetilde{U}_1 \neq \widetilde{U}_2$. Again, the continuous formulation allows extending the domain of the solution by introducing further design parameters such as the maneuvers' durations. In other words, the piecewise continuous solution still exists even though the critical separation between the maneuvers, $k_2 = 2n_2$, is chosen, if $\widetilde{U}_1 \neq \widetilde{U}_2$.

Similarly to the impulsive RT-RT strategy, when $k_2 \neq 2n_2$ the radial and tangential components of the maneuvers are correlated through the following relationships

$$\widetilde{U}_1 f_{y,1} + \widetilde{U}_2 f_{y,2} = \mu\Delta\delta a_{des} \tag{71}$$

$$f_{x,1}\sin\widetilde{U}_1 = f_{x,2}\sin\widetilde{U}_2. \tag{72}$$

In the case in which $\widetilde{U}_1 = \widetilde{U}_2$ and $\Delta\delta a_{des} = 0$, the difference of the x-component of thrust and the sum of the y-component of thrust must be zero in order to accomplish the reconfiguration.

Finally, it is noteworthy that another class of continuous solutions can be derived considering the following maneuvers' locations

$$\widehat{U}_1 = \overline{U}_x + k_1\pi\ ,\ \widehat{U}_2 = \widehat{U}_1 + k_2\pi\,. \tag{73}$$

The corresponding thrust magnitudes are omitted here for brevity. However they can be determined by solving the system of equations (31) for $f_{x,j}$ and $f_{y,j}$ with $j = 1, 2$. It is straightforward that a similar choice for the separation of the impulses leads to a feasible impulsive control solution.

3.2.4. T-T maneuver

When the in-plane reconfiguration is performed through a couple of pure tangential maneuvers, the analytical solutions of Eq. (31) (with $f_{x,j} = 0, j = 1, 2$) and Eq. (32) (with $\Delta v_{x,j} = 0, j = 1, 2$) do not exist. This means that an iterative algorithm is required to determine the thrust/impulses amplitude as well as the maneuvers' location over time. However, the problem might be simplified by recognizing that the unknowns $f_{y,j}$ and $\widehat{U}_j$ are linearly dependent through the Eqs. (31a-b) and, similarly, $\Delta v_{y,j}$ and U_j through the Eqs. (32a-b). In light of this, the magnitude of impulsive and extended maneuvers can be determined as a function of maneuvers' locations as follows

$$f_{y,1} = \frac{\beta W_c a_c n_c \left(\beta W_c \Delta\delta\lambda_{des} + \Delta\delta a_{des}\Lambda_c(u_T - \widehat{U}_2)\right)}{4\Lambda_c \widetilde{U}_1(\widehat{U}_1 - \widehat{U}_2)} \tag{74}$$

$$f_{y,2} = -\frac{\beta W_c a_c n_c \left(\beta W_c \Delta\delta\lambda_{des} + \Delta\delta a_{des}\Lambda_c(u_T - \widehat{U}_1)\right)}{4\Lambda_c \widetilde{U}_1(\widehat{U}_1 - \widehat{U}_2)} \tag{75}$$

$$\Delta v_{y,1} = \frac{a_c n_c \left(\beta W_c \Delta\delta\lambda_{des} + \Delta\delta a_{des}\Lambda_c(u_T - U_2)\right)}{2\Lambda_c(U_1 - U_2)} \tag{76}$$

$$\Delta v_{y,2} = -\frac{a_c n_c \left(\beta W_c \Delta\delta\lambda_{des} + \Delta\delta a_{des}\Lambda_c(u_T - U_1)\right)}{2\Lambda_c(U_1 - U_2)} \tag{77}$$

The maneuvers' locations, $\widehat{U}_j$ and U_j for finite-tme and impulsive schemes, can be obtained by substituting Eqs. (74) and (75) and Eqs. (76) and (77) into Eqs. (31c-d) and Eqs. (32c-d) respectively, and solving numerically. In this study the Matlab $fsolve$ routine provided by the Global Optimization Toolbox [33] and implementing the Levenberg–Marquardt algorithm [34] is used to solve Eqs. (31c-d) and Eqs. (32c-d). The iterative algorithm is initialized by analyzing the error functions, J_{con} and J_{imp}, defined as

follows

$$\boldsymbol{F}_{con} = \begin{bmatrix} \sum_{j=1}^{2} \left(\sin \widetilde{U}_j \cos \widehat{U}_j f_{y,j} \right) - \mu \Delta\delta e_{x,des} \\ \sum_{j=1}^{2} \left(\sin \widetilde{U}_j \sin \widehat{U}_j f_{y,j} \right) - \mu \Delta\delta e_{y,des} \end{bmatrix} = \begin{bmatrix} 0 \\ 0 \end{bmatrix} \tag{78}$$

$$J_{con} = \sqrt{\boldsymbol{F}_{con}^T \boldsymbol{F}_{con}} \tag{79}$$

and

$$\boldsymbol{F}_{imp} = \begin{bmatrix} \sum_{j=1}^{2} \left(2 \cos \widehat{U}_j \Delta v_{y,j} \right) - n_c a_c \Delta\delta e_{x,des} \\ \sum_{j=1}^{2} \left(2 \sin \widehat{U}_j \Delta v_{y,j} \right) - n_c a_c \Delta\delta e_{y,des} \end{bmatrix} = \begin{bmatrix} 0 \\ 0 \end{bmatrix} \tag{80}$$

$$J_{imp} = \sqrt{\boldsymbol{F}_{imp}^T \boldsymbol{F}_{imp}} \tag{81}$$

The above choice allows one to determine an initial guess that guaranteees the convergence of the numerical algorithm in a limited number of iterations.

3.3. Out-of-plane reconfiguration

The out-of-plane reconfiguration problem foresees the correction of only the relative inclination vector, thus it requires the solution of two nonlinear equations (i.e., the last two rows of Eq. (25) or Eq. (26) for piecewise continuous and impulsive strategies respectively) in $(1 + 1)n$ unknowns (i.e., the cross-track component of thrust or impulses vectors and the corresponding maneuver location).

. In order to achieve the desired x and y components of the relative inclination vector at the end of the maneuver, the control solution must include a component in the cross-track (z) direction. In fact, the only way to modify the difference of inclinations of the satellites' orbits (i.e., δi_x) is to provide a control action along the z-axis of the deputy RTN frame, as it is evident from the analysis of the linearized equations of relative motion (see Eq. (13)).

Assuming that a single time-finite cross-track maneuver is performed by the deputy satellite, i.e. $\boldsymbol{F}_1 = [0, 0, f_{z,1}]^T$, the equations governing the change of relative inclination vector are (see Eq. (25))

$$f_{z,1} \cos \hat{u}_1 \sin \tilde{u}_1 = \frac{W_c n_c a_c}{2} \Delta\delta i_{x,des}, \tag{82a}$$

$$2 f_{z,1} \frac{K_c T_c}{W_c} \Big((u_T - u_{1,f}) \cos \hat{u}_1 \sin \tilde{u}_1 + \sin \hat{u}_1 \sin \tilde{u}_1 - \sin u_{1,0} \tilde{u}_1 \Big) + \tag{82b}$$

$$f_{z,1} \sin \hat{u}_1 \sin \tilde{u}_1 = \frac{W_c n_c a_c}{2} \Delta\delta i_{y,des} \tag{82c}$$

where $u_{1,0}$ and $u_{1,f}$ are the mean argument of latitude of the chief orbit at the instants $t_{1,0}$ and $t_{1,f}$, respectively, whereas $\widehat{u}_1$ and $\widetilde{u}_1$ are defined in Eq. (29). Similarly, considering a single out-of-plane impulse, the change of mean ROE is governed by the following set of equations, [5]

$$\Delta v_{z,1} \cos u_1 = n_c a_c \Delta\delta i_{x,des} \tag{83a}$$

$$\left(\sin u_1 + 2\frac{K_c T_c}{W_c}(u_T - u_1)\cos u_1\right)\Delta v_{z,1} = n_c a_c \Delta\delta i_{y,des} \tag{83b}$$

As for the in-plane case, Eqs. (82a-b) reduce to Eqs. (83a-b) when $\tilde{u}_z \to 0$.

A full analytical solution does not exist in this case, neither for impulsive or extended maneuvers models. However, $\Delta v_{z,1}$ and $f_{z,1}$ can be computed as a function of the impulses' location and maneuver mid-point by inverting Eqs. (82a-b) respectively,

$$f_{z,1} = \frac{W_c n_c a_c}{2\cos\hat{u}_1 \sin\tilde{u}_1}\Delta\delta i_{x,des} \tag{84}$$

$$\Delta v_{z,1} = \frac{n_c a_c}{\cos\hat{u}_1}. \tag{85}$$

The location of the impulsive and extended maneuver can be found by substituting Eqs. (84) and (85) into Eqs. (82b) and (83b) to obtain the following transcendental expressions,

$$2\frac{K_c T_c}{W_c}\left(u_T - u_{1,f} + \tan\hat{u}_1 - \frac{\sin u_{1,0}\tilde{u}_1}{\cos\hat{u}_1 \sin\tilde{u}_1}\right) + \tan\hat{u}_1 = \frac{\Delta\delta i_{y,des}}{\Delta\delta i_{x,des}} \tag{86}$$

$$2\frac{K_c T_c}{W_c}(u_T - u_1) + \tan u_1 = \frac{\Delta\delta i_{y,des}}{\Delta\delta i_{x,des}} \tag{87}$$

Eqs. (86) and (87) can be numerically solved by using an iterative algorithm. The results obtained with the Matlab built-in routine *fzero* are presented in Section 4. A good initial guess that guarantees a fast convergence of the iterative approach is $\hat{u}_{1,z} = u_{1,z} = \tan^{-1}(\Delta\delta i_{y,des}/\Delta\delta i_{x,des})$, which is the location of maneuver corresponding to the single impulse maneuver scheme for unperturbed orbits, as proved in [5] and [23]. However, a graphical method is used in this study to define the initial guess for the *fzero* solver. In further details the fololwing error functions,

$$J_{cont} = 2\frac{K_c T_c}{W_c}\left(u_T - u_{1,f} + \tan\hat{u}_1 - \frac{\sin u_{1,0}\tilde{u}_1}{\cos\hat{u}_1 \sin\tilde{u}_1}\right) + \tan\hat{u}_1 - \frac{\Delta\delta i_{y,des}}{\Delta\delta i_{x,des}} \tag{88}$$

$$J_{imp} = 2\frac{K_c T_c}{W_c}(u_T - u_1) + \tan u_1 - \frac{\Delta\delta i_{y,des}}{\Delta\delta i_{x,des}} \tag{89}$$

are computed varying the variables $\hat{u}_1$ and u_1, and the corresponding zeros are graphically determined to be used as initial guess for the numerical solver.

4. Numerical validation of the control solutions

In this section the relative trajectories obtained using the developed control solutions are presented, pointing out their performances in terms of maneuver cost and accuracy. Fig. 2 illustrates the simulation setup exploited for the validation of the proposed maneuvering solutions.

First, the initial mean orbit elements of the chief and the mean ROE state are set. Then, the initial mean orbit elements of the deputy are computed using the identities (8). A numerical

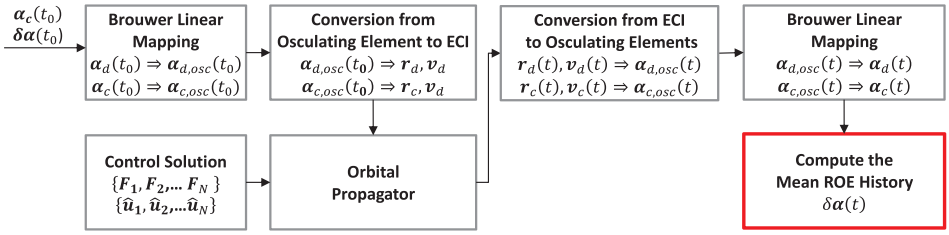

Fig. 2. Scheme for numerical validation.

propagator including the Earth's oblateness J_2 effects is used to obtain the history of position and velocity of chief and deputy spacecraft expressed in the Earth Centered Inertial (ECI) reference frame (J2000). The initial Cartesian states of both satellites are derived using the linear mapping developed by Brouwer and Lyddane to transform the mean orbit elements into osculating and the nonlinear relations between Cartesian state and osculating elements [35–37]. The control thrust profile is projected in ECI and added as external accelerations to the deputy's motion. After the simulation, the absolute position and velocity of the spacecraft are converted into the mean orbit elements to compute the accuracy at the end of the maneuver, defined as

$$\varepsilon_{\Delta\delta\alpha_k}(T) = \frac{\Delta\delta\alpha_k^{num}(T) - \Delta\delta\alpha_{k,des}}{|\Delta\delta\alpha_{k,des}|} a_c(t_0)\,, \quad k = 1, \ldots, 6. \tag{90}$$

To compare the maneuvering performances deriving from impulsive and finite-time control strategies, the instantaneous velocity change computed by the impulsive scheme, $\Delta v_{j,i}$ with $i = x, y, z$, is spread over a finite-time maneuver through the following relationship

$$f_{j,i}^{imp} = \frac{\Delta v_{j,i} W_c}{2\tilde{u}_j} \tag{91}$$

In fact, the impulsive scheme implies an instantaneous variation of the deputy velocity with no change of position, i.e. an instantaneous change of mean ROE. Then, the impulsive approach can be adopted only when the firing interval is small as compared with the orbital period, otherwise it might fail in achieving the desired level of accuracy. However, many real applications might need a long time maneuver in order to meet some specific constraints, e.g. the maximum thrust provided by onboard actuators, requiring the $\Delta v_{j,i}$-to-$f_{j,i}^{imp}$ conversion in Eq. (91).

In order to verify the effectiveness of the developed control solutions two test cases are carried out, one for in-plane and the other for out-of-plane reconfiguration problem defined in the previous sections.

4.1. In-plane reconfiguration control problem

This section presents the trajectories obtained using the 2- and 3-maneuver strategies described in Section 3.2. The initial conditions used in the simulations below are listed in Tables 1 and 2 (see first row), along with the desired mean ROE vector. Note that the initial mean state of the chief is expressed in terms of quasi-nonsingular orbital elements, [26]. The chief orbit is assumed to be circular at 200 km of altitude and the reconfiguration maneuver lasts 6 chief orbital periods, i.e. $u_T = 12\pi$ corresponding to $T = 528.6$ (min), with the initial

Table 1
Initial mean chief orbit.

a_c (km)	e_{xc} (dim)	e_{yc} (dim)	i_c (deg)	Ω_c (deg)	$f_{c,0}$ (deg)
6578	0	0	8	0	0

Table 2
Initial and desired mean relative orbits.

	$a_c\delta a$ (m)	$a_c\delta\lambda$ (m)	$a_c\delta e_x$ (m)	$a_c\delta e_y$ (m)
Initial relative orbit, $\delta\boldsymbol{\alpha}_0$	30	-11×10^3	0	−50
Desired relative orbit, $\delta\boldsymbol{\alpha}_{des}$	0	-10.5×10^3	45	70

Table 3
Design parameters for in-plane continuous strategies.

	$2\tilde{u}_1$ (rad)	$2\tilde{u}_2$ (rad)	$2\tilde{u}_3$ (rad)	T (orbits)	k_j (dim)
R-R	π	1.5π	0	6	[1,3]
RT-RT	π	1.5π	0	6	[1,3]
T-T	π	1.5π	0	6	-
T-T-T	$\pi/2$	π	1.5π	6	[1,4,7]

mean argument of latitude equal to zero, i.e. $u_0 = 0$. The values of $\delta\boldsymbol{\alpha}_0$ and $\delta\boldsymbol{\alpha}_{des}$ lead to $a_c\Delta\delta\hat{\boldsymbol{\alpha}}_{des} = a_c[\Delta\delta a_{des}, \Delta\delta\lambda_{des}, \Delta\delta e_{x,des}, \Delta\delta e_{y,des}]^T = [-0.03, 2.2, 0.0394, 0.11968]^T$ (km).

Table 3 reports the durations, $\tilde{u}_j$ with $j = 1, ..., 3$, as well as the locations, k_j, used in the analyses for all maneuvers' combinations, i.e. R-R, RT-RT, T-T, and T-T-T. Note that the parameters k_j are not reported in the table for the T-T in-plane maneuver. In fact, this control scheme does not enable finding the maneuver location analytically, as discussed in Section 3.2.4.

Fig. 3 shows the mean ROE state variation over time for all four in-plane extended maneuvers. Note that the ROE are scaled by the final desired ROE correction as

$$\varepsilon_{\Delta\delta\alpha_k}(t) = \frac{\Delta\delta\alpha_k^{num}(t) - \Delta\delta\alpha_{k,des}}{|\Delta\delta\alpha_{k,des}|} a_c(t_0)\,, \quad k = 1, \ldots, 6. \tag{92}$$

From the figure, the piecewise continuous solutions allow achieving the desired relative configuration in the defined interval of time. Note that the R-R scheme is not able to control the variation of mean relative semi-major axis. With reference to Eq. (31), it is clear that an along-track maneuver is necessary to modify the orbital energy of the deputy and, then, the mean relative semi-major axis. In addition, let us recall that the maneuvers' locations associated with the T-T strategy are computed using the Matlab routine *fsolve*, as discussed in Section 3.2.4. The initial guess for the iterative algorithm was determined by analyzing the error functions, J_{con} and J_{imp} reported in Eqs. (79) and (81). Fig. 4(a) and (b) depict J_{con} and J_{imp} when $\widehat{U}_1, \widehat{U}_2 \in [Cu_T + \tilde{U}_1, u_T - \tilde{U}_2]$ with $\widehat{U}_2 > \widehat{U}_1$. The red point indicates the selected initial guess and corresponds to $\widehat{U}_{1,ig} = 16.63$ (rad) and $\widehat{U}_{2,ig} = 21.51$ (rad) for both extended and impulsive T-T maneuvers. This choice allows the iterative algorithm to converge in 14 iterations.

Fig. 5 illustrates the evolution of the relative position projected on the along-track/cross-track plane of the RTN reference plane. In the same figure the extended maneuvers are

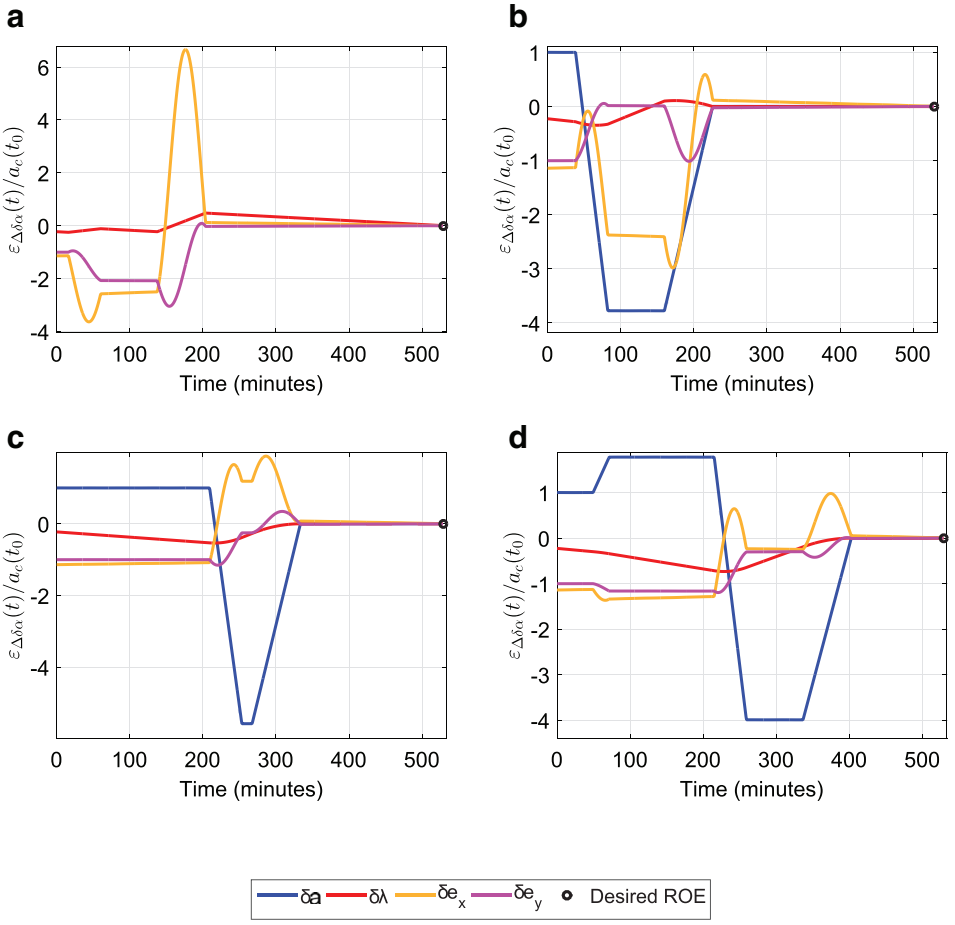

Fig. 3. Accuracy of the in-plane extended maneuvers: (a) R-R, (b) RT-RT, (c) T-T, (d) T-T-T.

depicted (see magenta, green and cyan markers corresponding to the first, the second and the third maneuver). The initial and the aimed relative positions are indicated by the red and black markers, respectively. Finally, Fig. 6 shows the thrust profile along the x and y directions of the RTN reference frame. It is worth noting that the radial maneuvers provide the highest values of accelerations (e.g., the R-R maneuver requires a maximum acceleration of $|f_x^{max}| = 2.62 \times 10^{-7}$ (km/s^2), whereas RT-RT requires a maximum acceleration of $|f_x^{max}| = 0.93 \times 10^{-7}$ (km/s^2)).

The results in terms of maneuver cost are summarized in Tables 4 and 5 for finite-time and impulsive solutions, respectively. Given the thrust value from the piecewise control model, the total maneuver delta-V is computed using the following expression

$$\Delta v_T = \sum_{j=1}^{n} \frac{2f_{x,j}\widetilde{u}_j}{W_c} + \frac{2f_{y,j}\widetilde{u}_j}{W_c} + \frac{2f_{z,j}\widetilde{u}_j}{W_c}. \tag{93}$$

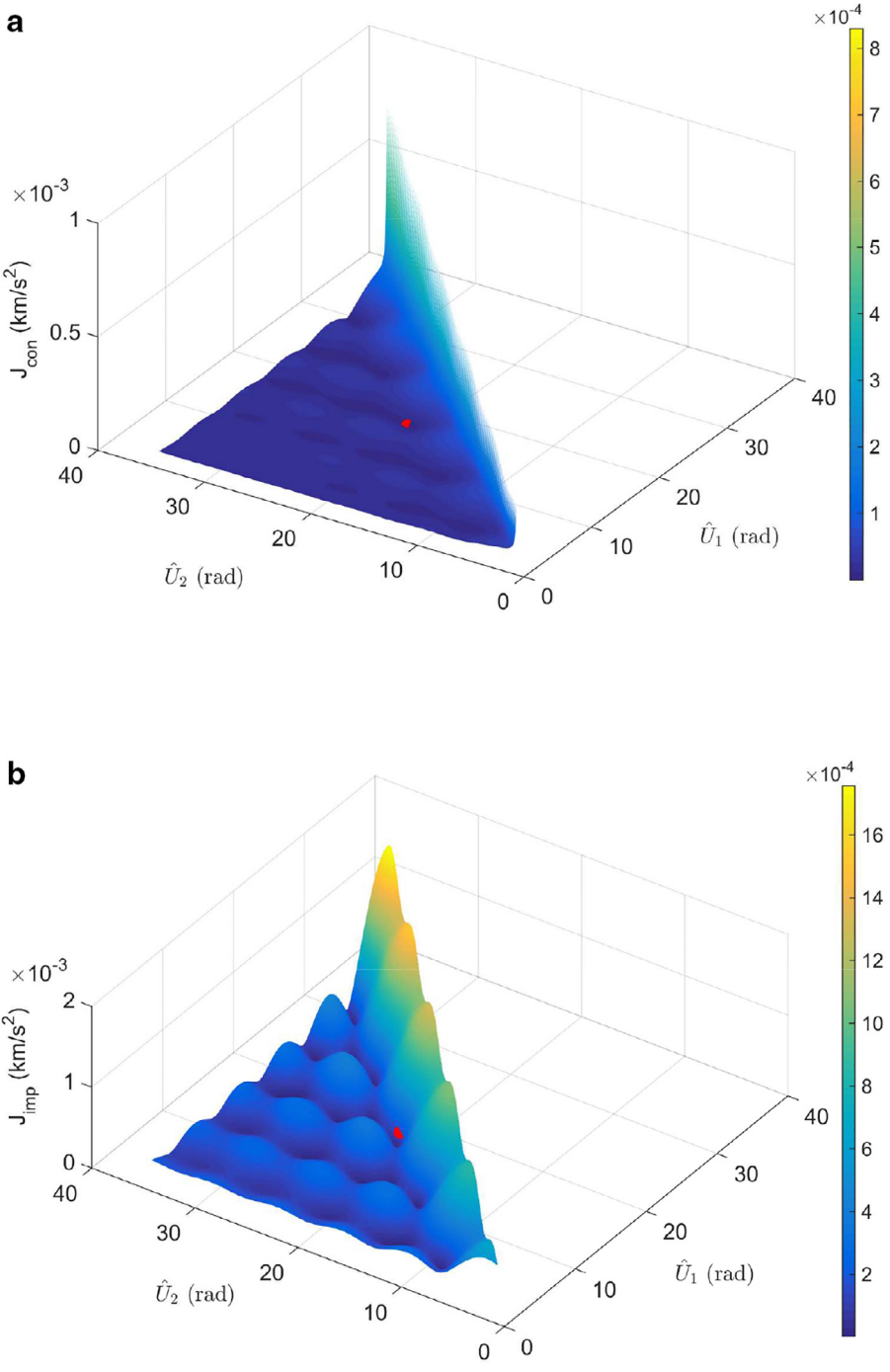

Fig. 4. Error functions for T-T solution derivation: (a) J_{con}, (b) J_{imp}.

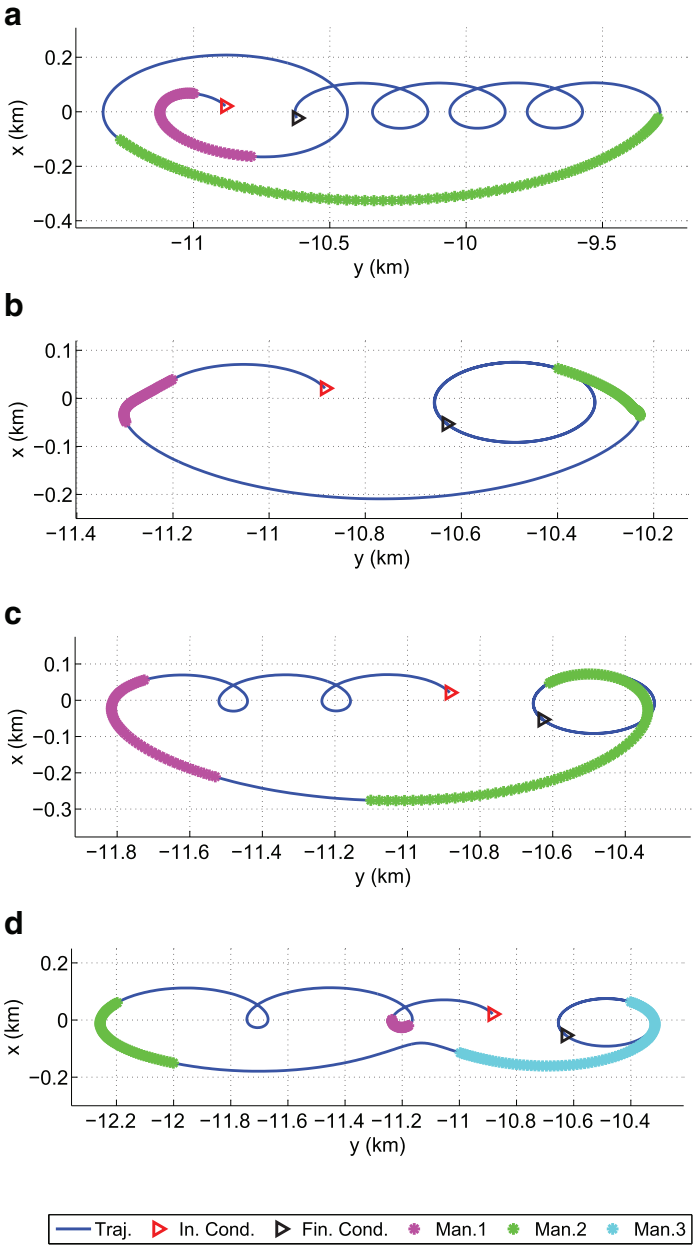

Fig. 5. $x - y$ trajectory of the in-plane extended maneuvers: (a) R-R, (b) RT-RT, (c) T-T, (d) T-T-T. (For interpretation of the references to color in this figure, the reader is referred to the web version of this article.)

From the results summarized in Tables 4 and 5, it can be observed that the finite-duration maneuver solutions require higher delta-V than the corresponding impulsive ones, except for the R-R scheme that provides the same delta-V for continuous and impulsive approaches, as proved in Section 3.2.2. In addition, it is noteworthy that the maximum cost is given

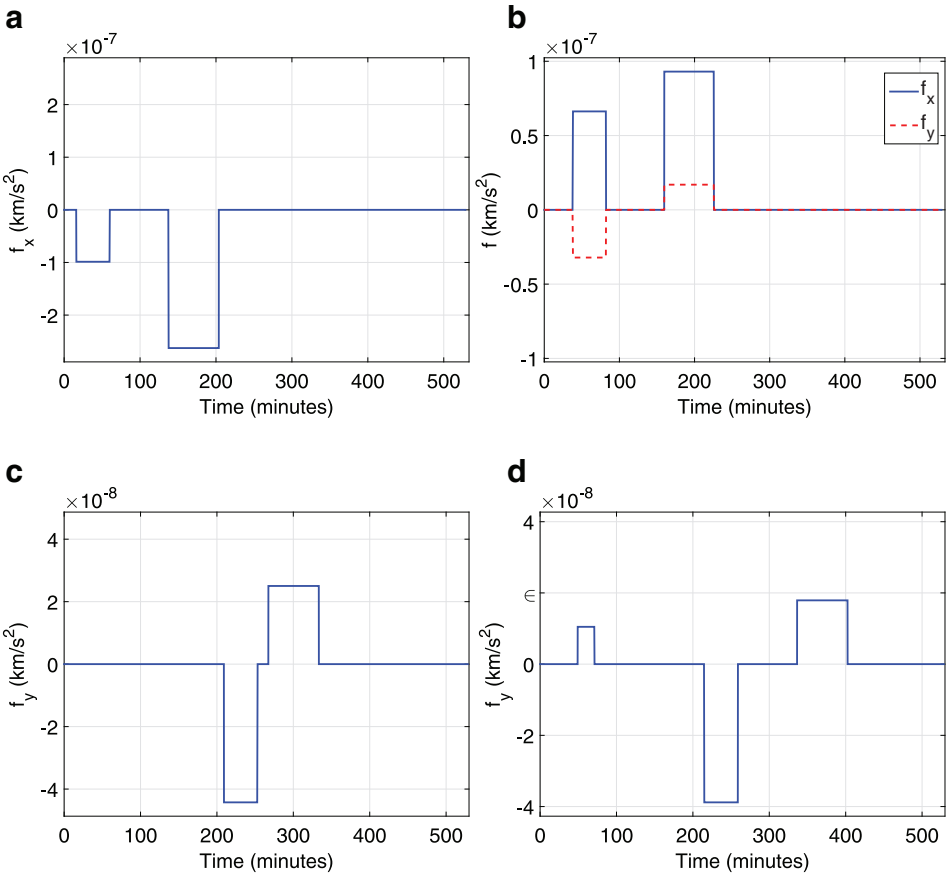

Fig. 6. Thrust profile of the in-plane extended maneuvers: (a) R-R, (b) RT-RT, (c) T-T, (d) T-T-T.

Table 4
Costs of the in-plane extended maneuvers.

		R-R	RT-RT	T-T	T-T-T
$\Delta v_{x,1}$	(m/s)	−0.261	0.175	0	0
$\Delta v_{x,2}$	(m/s)	−1.04	0.369	0	0
$\Delta v_{y,1}$	(m/s)	0	−0.0849	−0.117	0.0138
$\Delta v_{y,2}$	(m/s)	0	0.0671	0.0992	−0.103
$\Delta v_{y,3}$	(m/s)	0	0	0	0.0710
Δv_T	(m/s)	1.30	0.696	0.216	0.187

by 2-maneuver radial strategy, wheras the minimum delta-V is obtained by the 3-maneuver tangential scheme, for both impulsive and finite-time approaches.

Finally, Table 6 shows a comparison in terms of accuracy between the piecewise continuous and impulsive solutions. Here, the impulses, $\Delta v_{x,j}$ and $\Delta v_{y,j}$, given by the impulsive solutions are transformed in a finite-time maneuver through Eq. (91). The last column in Table 6 lists

Table 5
Costs of the in-plane impulsive maneuvers.

		R-R	RT-RT	T-T	T-T-T
$\Delta v_{x,1}$	(m/s)	-0.577	-3.37×10^{-3}	0	0
$\Delta v_{x,2}$	(m/s)	-0.726	-3.37×10^{-3}	0	0
$\Delta v_{y,1}$	(m/s)	0	-0.0462	-0.105	-0.0181
$\Delta v_{y,2}$	(m/s)	0	0.0284	0.0869	-0.0281
$\Delta v_{y,3}$	(m/s)	0	0	0	0.0284
Δv_T	(m/s)	1.30	0.0813	0.192	0.0746

Table 6
In-plane accuracies of extended and impulsive maneuvers.

	$\lvert\varepsilon_{\Delta\delta a}(T)\rvert$ (m)	$\lvert\varepsilon_{\Delta\delta\lambda}(T)\rvert$ (m)	$\lvert\varepsilon_{\Delta\delta e_x}(T)\rvert$ (m)	$\lvert\varepsilon_{\Delta\delta e_y}(T)\rvert$ (m)	ε_T (m)
			Extended maneuvers		
R-R	-	1.84×10^{-3}	1.30×10^{-3}	1.49×10^{-3}	2.70×10^{-3}
RT-RT	1.55×10^{-3}	2.37×10^{-3}	4.86×10^{-3}	5.30×10^{-4}	5.64×10^{-3}
T-T	1.50×10^{-3}	1.11×10^{-3}	4.72×10^{-3}	2.32×10^{-4}	5.08×10^{-3}
T-T-T	1.51×10^{-3}	1.12×10^{-3}	4.74×10^{-3}	3.25×10^{-4}	5.11×10^{-3}
			Impulsive maneuvers		
R-R	-	1.70×10^{-3}	2.00	1.99	2.82
RT-RT	1.48×10^{-3}	1.11×10^{-3}	4.64×10^{-1}	4.92×10^{-1}	6.76×10^{-1}
T-T	1.51×10^{-3}	1.12×10^{-3}	7.47×10^{-1}	5.54×10^{-1}	9.30×10^{-1}
T-T-T	1.49×10^{-3}	1.12×10^{-3}	4.23×10^{-1}	4.25×10^{-1}	6.00×10^{-1}

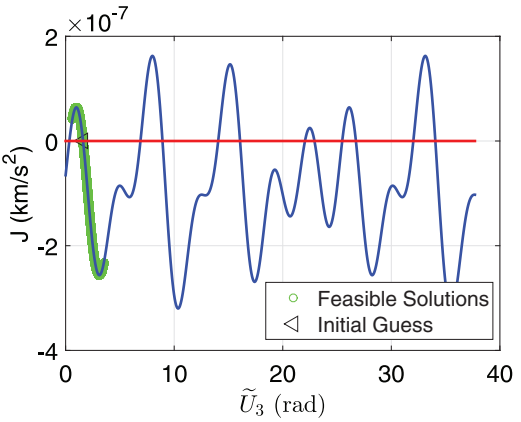

Fig. 7. Error function for the derivation of constrained T-T-T solution.

the total error defined as

$$\varepsilon_T = \sqrt{(|\varepsilon_{\Delta\delta a}(T)|)^2 + (|\varepsilon_{\Delta\delta\lambda}(T)|)^2 (|\varepsilon_{\Delta\delta e_x}(T)|)^2 + (|\varepsilon_{\Delta\delta e_y}(T)|)^2}. \tag{94}$$

The piecewise control solution provides an accuracy 2 orders of magnitude greater than the corresponding impulsive solution. More specifically, the impulsive strategy produces a high error on the final relative eccentricity, while it provides the same accuracy level on

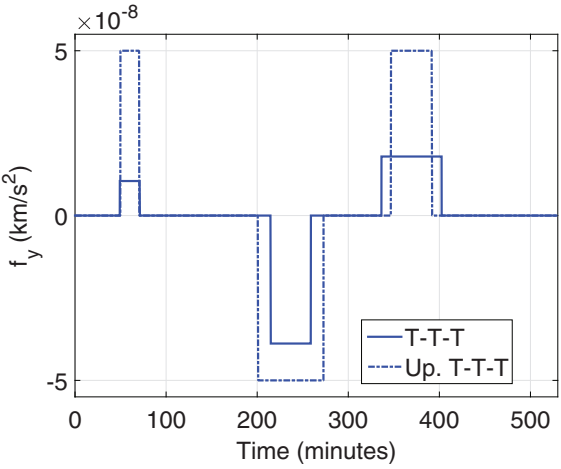

Fig. 8. Updated control thrust profile.

the mean relative semi-major axis and longitude. This fact can be justified by looking at the equations governing the mean ROE variation for finite-time and impulsive models, Eqs. (31) and (32) respectively. In fact, substituting Eq. (91) into Eq. (31), Eqs. (31a-b) and Eqs. (32a-b) coincide. On the contrary, the equations governing the change of relative eccentricity vector for both models are not the same when the mapping (91) is used.

4.1.1. T-T-T maneuver with thrust constraint

This section is meant to present the results obtained by the T-T-T control strategy with thrust constraint discussed in Section 3.2.1. Without affecting the generality of the method, the scenario described in Section 4.1 (see Tables 1 and 2) is considered. The analytical approach gives the thrust profile showed in Fig. 10(d), with the accelerations $f_{y,1} = 1.047 \times 10^{-8}$ (km/s^2), $f_{y,2} = -3.88 \times 10^{-8}$ (km/s^2), and $f_{y,3} = 1.791 \times 10^{-8}$ (km/s^2) located at $\widehat{U}_1 = \arctan(\frac{\Delta\delta e_{y,des}}{\Delta\delta e_{x,des}}) + \pi$ (rad), $\widehat{U}_2 = \widehat{U}_1 + 4\pi$ (rad), and $\widehat{U}_3 = \widehat{U}_1 + 7\pi$ (rad). The updated T-T-T control scheme is computed by numerically solving Eq. (48) through the Matlab built-in routine *fzero*. Fig. 7 illustrates the error function obtained imposing $f_{max} = 5 \times 10^{-8}$ km/s^2 and $\widetilde{U}_3^{up} \in (0, u_T)$. The green markers in the figure indicate the values of $\widetilde{U}_3$ corresponding to the feasible solutions (see Eq. (51)). The initial guess $\widetilde{U}_{3,ig}^{up} = 1.605$ (rad) allows *fzero* routine to converge in 6 iterations and leads to the values of maneuvers' durations $\widetilde{U}_1^{up} = 0.737$ (rad), $\widetilde{U}_2^{up} = 2.552$ (rad) and $\widetilde{U}_3^{up} = 1.605$ (rad), corresponding to $\Delta t^{up} = [\Delta t_1{}^{up}, \Delta t_2{}^{up}, \Delta t_3{}^{up}] = [20.71, 71.77, 45.14]$ (min). Fig. 8 shows the updated thrust profile (dashed line) along with the analytical control solution (solid line). From this figure, it is clear that the updated T-T-T maneuver requires a higher delta-V than the analytical solution, i.e. $\Delta v_T^{up} = 0.412$ (m/s). Fig. 9 shows the trajectories projected in the $x - y$ plane of the RTN reference plane for updated (dashed line) and analytical (solid line) solutions. Finally, Table 7 reports the value of maneuver accuracy corresponding to the new control solution. As can be observed, the updated control solution guarantees the achievement of the desired ROE correction with the same accuracy of the analytical one.

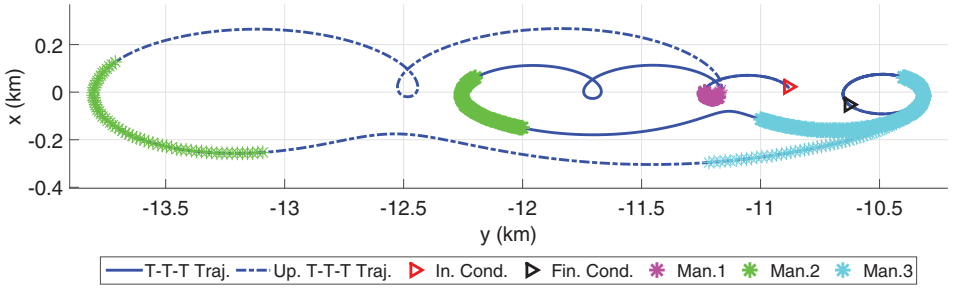

Fig. 9. $x-y$ trajectory of the updated T-T-T extended maneuvers.

Table 7
Accuracy for updated T-T-T maneuver scheme.

	$\varepsilon_{\Delta\delta a}$ (m)	$\varepsilon_{\Delta\delta\lambda}$ (m)	$\varepsilon_{\Delta\delta e_x}$ (m)	$\varepsilon_{\Delta\delta e_y}$ (m)	ε_T (m)
T-T-T	1.47e-3	1.09e-3	4.48e-3	2.37e-4	4.84e-3

Table 8
Initial mean chief orbit.

a_c (km)	e_{xc} (dim)	e_{yc} (dim)	i_c (deg)	Ω_c (deg)	f_c (deg)
6828	0	0	40	0	0

Table 9
Initial and desired mean relative orbits.

	$a_c\delta i_x$ (m)	$a_c\delta i_y$ (m)
Initial relative orbit, $\delta\boldsymbol{\alpha}_0$	5	70
Desired relative orbit, $\delta\boldsymbol{\alpha}_{des}$	40	120

4.2. Out-of-plane reconfiguration control problem

In this section, the results relative to the out-of-plane reconfiguration obtained by a single cross-track maneuver (N) are presented. Here, the chief moves on a circular orbit at an altitude of 450 (km) and an inclination of $i = 40$ (deg) (see Table 8). The reconfiguration maneuver has to occur in 6 chief orbital periods, i.e. $u_T = 12\pi$ corresponding to $T = 560.4$ (min). The initial mean argument of latitude is assumed to be zero, i.e. $u_0 = 0$. The final desired mean ROE is listed in Table 9. Accordingly, the values of $\delta\boldsymbol{\alpha}_0$ and $\delta\boldsymbol{\alpha}_{des}$ yield the correction of mean ROE, $a_c\Delta\delta\hat{\boldsymbol{\alpha}}_{des} = a_c[\Delta\delta i_{x,des}, \Delta\delta i_{y,des}]^T = [35, 49.9]^T$ (m). Here, a maneuver duration of 70.05 (min) is assumed, corresponding to $\tilde{u}_1 = 1.5\pi$ (rad). As discussed in Section 3.3, the location of the cross-track maneuver has to be determined by solving numerically Eqs. (82) and (83) for finite-time and impulsive methodologies respectively. Recall that the Matlab built-in routine *fzero* is exploited to solve the aforementioned nonlinear equations in the unknows $\hat{u}_j$ and u_j. A parametric analysis of the error functions reported in Eq. (86) and Eq. (87) is carried out yielding $\hat{u}_{1,ig} = u_{1,ig} = 16.65$ (rad).

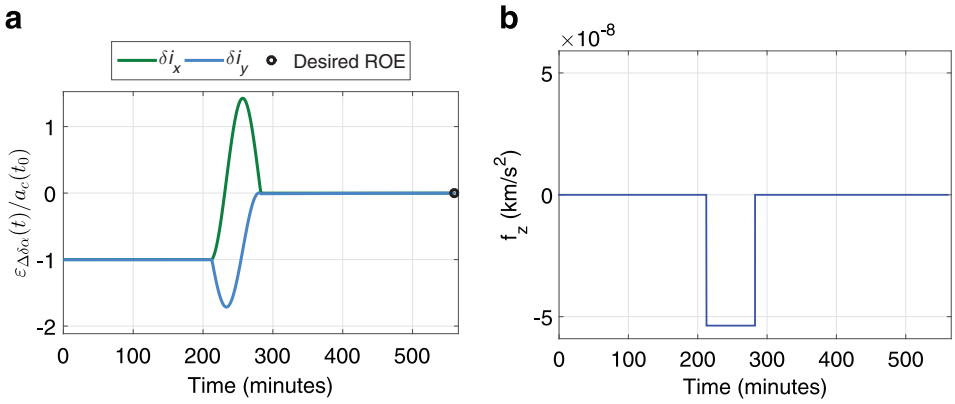

Fig. 10. Accuracy (a) and thrust profile (b) for N extended maneuver.

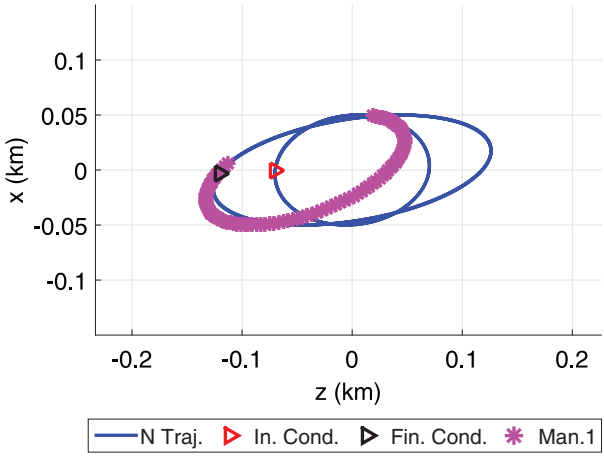

Fig. 11. $z-x$ trajectory of the out-of-plane (N) extended maneuver.

Fig. 10 depicts the mean ROE variation over the maneuver interval (Fig. 10(a)) and the corresponding thrust profile (Fig. 10(b)) along the cross-track direction of the RTN reference frame. The obtained amplitude of finite-time maneuver is $f_{z,1} = -5.368 \times 10^{-8}$ (km/s^2). Fig. 11 illustrates the trajectory projected on the coss-track/radial plane of the RTN reference frame, along with its location. The initial and the aimed relative positions are indicated by the red and black markers, respectively. The derived piecewise continuous and impulsive solutions provide a delta-V of $\Delta v_z = -2.2563 \times 10^{-1}$ (m/s) and $\Delta v_z = -6.7801 \times 10^{-2}$ (m/s) respectively. Again, the impulsive solution is less demanding in terms of delta-V. However, when the impulse is converted into a finite-duration maneuver through Eq. (91), a decreased accuracy is achieved as compared with that obtained using the finite-time model. As showed by the results listed in Table 10, the impulsive approach provides an error at the end of the maneuvering interval, $\varepsilon_T = \sqrt{(|\varepsilon_{\Delta\delta i_x}(T)|)^2 + (|\varepsilon_{\Delta\delta i_y}(T)|)^2}$, two orders of magnitudes higher than the one given by the finite-time strategy.

Table 10
Out-of-plane accuracies of extended and impulsive maneuvers.

	$\lvert\varepsilon_{\Delta\delta i_x}(T)\rvert$ (m)	$\lvert\varepsilon_{\Delta\delta i_y}(T)\rvert$ (m)	ε_T (m)
	Extended maneuver		
N	1.07×10^{-3}	7.86×10^{-4}	1.32×10^{-3}
	Impulsive maneuver		
N	7.00×10^{-1}	7.00×10^{-1}	9.90×10^{-1}

5. Conclusion

This paper addressed the spacecraft formation reconfiguration problem over a limited and defined interval of time by using impulsive and extended maneuver strategies, in near-circular J2-perturbed orbits. The analytical impulsive and piecewise continuous control solutions for in-plane and out-of-plane reconfigurations (i.e. the maneuvers' locations and the corresponding magnitudes) have been derived by inverting the closed-form solution of relative dynamics, parameterized through the relative orbit elements. More specifically, 2- and 3-maneuver schemes have been investigated for the in-plane reconfiguration, whereas single maneuver strategy have been considered for the out-of-plane reconfiguration.

It has been rigorously proven that the piecewise continuous solutions converge to the impulsive one when the durations of the maneuvers tend to zero. Moreover, special focus has been given to the range of applicability of the proposed solutions. It has been observed that the extended maneuver approach allows increasing the domain of the solution by considering the maneuver duration as additional design paramenter.

Finally, numerical simulations have been carried out to assess the effectiveness of the derived solutions. A critical comparison of continuous and impulsive schemes have been performed to show the benefits of considering the dynamical effect of thruster firing in the derivation of the control solution. It has been showed that, while the impulsive strategy requires lower delta-V for formation maneuvering, the piecewise continuous approach always guarantees a higher accuracy, reducing the relative positon and velocity errors at the end of reconfiguration maneuver. In further details, the piecewise control solution provides an accuracy 2 orders of magnitude greater than the corresponding impulsive one. Then, the thrust profile can be computed according to the new analytical piecewise control solution that, thanks to its negligible computational burden, is ideally suited for an onboard implementation.

Possible future works include a thorough analysis of optimality of the derived control solutions as well as the extension of such piecewise continuous solutions for orbits with an arbitrary eccentricity, perturbed by the atmospheric drag and solar radiation pressure.

Acknowledgments

The authors would like to thank the United States Air Force Research Laboratory, Space Vehicles Directorate, for sponsoring this investigation under contract FAA9453-16-C-0029.

Appendix A. Control influence matrix Γ

The elements of control influence matrix Γ_F (see Eq. (6)) are

$\gamma_{13} = \gamma_{41} = \gamma_{51} = \gamma_{52} = \gamma_{62} = 0$

$$
\begin{aligned}
\gamma_{11} &= \frac{2e_d s_{f_d}}{n_d \eta_d a_c}, \qquad \gamma_{12} = \frac{2(1+e_d c_{f_d})}{n_d \eta_d a_c} \\
\gamma_{21} &= -\frac{\eta_d e_d c_{f_d}}{a_d n_d (1+\eta_d)} - \frac{2\eta_d^2}{a_d n_d (1+e_d c_{f_d})} \\
\gamma_{22} &= -\frac{\eta_d e_d [(2+e_d c_{f_d}) s_{f_d}]}{a_d n_d (1+\eta_d)(1+e_d c_{f_d})} \\
\gamma_{23} &= -\frac{\eta s_{\theta_d} (c_{i_c} - c_{i_d})}{a_d n_d (1+e_d c_{f_d}) s_{i_d}} \\
\gamma_{31} &= \frac{\eta_d s_{\theta_d}}{a_d n_d}, \qquad \gamma_{32} = \frac{\eta_d (2+e_d c_{f_d}) c_{\theta_d} + \eta_d e_{xd}}{a_d n_d (1+e_d c_{f_d})} \\
\gamma_{33} &= \frac{\eta_d e_{yd} s_{\theta_d} cotg(i_d)}{a_d n_d (1+e_d c_{f_d})} \\
\gamma_{41} &= -\frac{\eta_d c_{\theta_d}}{a_d n_d}, \qquad \gamma_{42} = \frac{\eta_d (2+e_d c_{f_d}) s_{\theta_d} + \eta_d e_{yd}}{a_d n_d (1+e_d c_{f_d})} \\
\gamma_{43} &= -\frac{\eta_d e_{xd} s_{\theta_d} \cot(i_d)}{a_d n_d (1+e_d c_{f_d})} \\
\gamma_{53} &= \frac{\eta_d s_{\theta_d}}{a_d n_d (1+e_d c_{f_d})}, \quad \gamma_{63} = \frac{\eta_d c_{\theta_d} s_{i_c}}{a_d n_d (1+e_d c_{f_d}) s_{i_d}}
\end{aligned}
\tag{A.1}
$$

where f_d and θ_d represent the true anomaly and true argument of latitude of the deputy respectively.

References

[1] S.S. Vaddi, K.T. Alfriend, S.R. Vadali, P. Sengupta, Formation establishment and reconfiguration using impulsive control, J. Guidance Control Dyn. 28 (2) (2005) 262–268, doi:10.2514/1.6687.

[2] K. Alfriend, S. Vadali, P. Gurfil, J. How, L. Breger, Spacecraft Formation Flying: Dynamics, Control and Navigation, Elsevier Astrodynamics Series, Elsevier Science, 2009. https://books.google.com/books?id=6EidgM-aX_oC.

[3] G. Gaias, S. D'Amico, Impulsive maneuvers for formation reconfiguration using relative orbital elements, J. Guidance Control Dyn. 38 (6) (2015) 1036–1049, doi:10.2514/1.G000189.

[4] Y. Ichimura, A. Ichikawa, Optimal impulsive relative orbit transfer along a circular orbit, J. Guidance Control Dyn. 31 (4) (2008) 1014–1027, doi:10.2514/1.32820.

[5] M. Chernick, S. D'Amico, New closed-form solutions for optimal impulsive control of spacecraft relative motion, in: Proceedings of the AIAA/AAS Astrodynamics Specialist Conference, AIAA SPACE Forum, 2016, doi:10.2514/6.2016-5659.

[6] M.M. Armellin Roberto, A.E. Finzi, Optimal formation flying reconfiguration and station keeping maneuvers using low thrust propulsion, in: Proceedings of the 18th International Symposium on Space Flight Dynamics (ESA SP-548), 2004, pp. 429–434.

[7] G.T. Huntington, D. Benson, A.V. Rao, Optimal configuration of tetrahedral spacecraft formations, J. Astronaut. Sci. 55 (2) (2007) 141–169, doi:10.1007/BF03256518.

[8] G.S. Aoude, J.P. How, I.M. Garcia, Two-stage path planning approach for solving multiple spacecraft reconfiguration maneuvers, J. Astronauti. Sci. 56 (4) (2008) 515–544, doi:10.1007/BF03256564.

[9] L.M. Steindorf, S. D'Amico, J. Scharnagl, F. Kempf, K. Schilling, Constrained low-thrust satellite formation-flying using relative orbit elements, in: Proceedings of the 27th AAS/AIAA Space Flight Mechanics Meeting, San Antonio, Texas, 2017. https://people.stanford.edu/damicos/sites/default/files/sfm2017_steindorfdamico.pdf.

[10] J. Bae, Y. Kim, Adaptive controller design for spacecraft formation flying using sliding mode controller and neural networks, J. Frankl. Inst. 349 (2) (2012) 578–603, doi:10.1016/j.jfranklin.2011.08.009.

[11] A. Imani, M. Bahrami, Optimal sliding mode control for spacecraft formation flying in eccentric orbits, in: Proceedings of the Institution of Mechanical Engineers Part I: Journal of Systems and Control Engineering, 2013, pp. 474–481, doi:10.1177/0959651813477786.
[12] G. Di Mauro, P. Di Lizia, M. Lavagna, Control of relative motion via state-dependent Riccati equation technique, Adv. Astronaut. Sci. 142 (4) (2012) 909–928.
[13] Y.-Y. Chen, Y. Zhang, C.-L. Liu, P. Wei, Coordinated orbit-tracking control of second-order non-linear agents with directed communication topologies, Int. J. Syst. Sci. 47 (16) (2016) 3929–3939, doi:10.1080/00207721.2016.1139759.
[14] H.-C. Cho, S.-Y. Park, K.-H. Choi, Application of analytic solution in relative motion to spacecraft formation flying in elliptic orbit, J. Astron. Space Sci. 25 (3) (2008) 255–266, doi:10.5140/JASS.2008.25.3.255.
[15] H.-C. Cho, S.-Y. Park, Analytic solution for fuel-optimal reconfiguration in relative motion, J. Optim. Theory Appl. 141 (3) (2009) 495–512, doi:10.1007/s10957-008-9482-3.
[16] S. Lee, S.-Y. Park, Approximate analytical solutions to optimal reconfiguration problems in perturbed satellite relative motion, J. Guidance Control Dyn. 34 (4) (2011) 1097–1111, doi:10.2514/1.52283.
[17] S.-M. Yoo, S. Lee, C. Park, S.-Y. Park, Spacecraft fuel-optimal and balancing maneuvers for a class of formation reconfiguration problems, Adv. Space Res. 52 (8) (2013) 1476–1488, doi:10.1016/j.asr.2013.07.019.
[18] C. Park, J.H. Yang, D.J. Scheeres, Optimal formation reconfigurations subject to hill three-body dynamics, J. Guidance Control Dyn. 37 (2) (2014) 700–704, doi:10.2514/1.60944.
[19] M. Lawn, G. Di Mauro, R. Bevilacqua, Guidance solutions for spacecraft planar rephasing and rendezvous using input shaping control, J. Guidance Control Dyn. (2017) 1–13, doi:10.2514/1.G002910.
[20] M.K.B. Larbi, E. Stoll, Spacecraft formation control using analytical finite-duration approaches, CEAS Space J. (2017) 1–15, doi:10.1007/s12567-017-0162-8.
[21] K.T. Alfried, H. Yan, Evaluation and comparison of relative motion theories, J. Guidance Control Dyn. 28 (2) (2005) 254–261, doi:10.2514/1.6691.
[22] J. Sullivan, S. Grimberg, S. D'Amico, Comprehensive survey and assessment of spacecraft relative motion dynamics models, J. Guidance Control Dyn. 40 (82) (2014) 1837–1859, doi:10.2514/1.G002309.
[23] G. Di Mauro, R. Bevilacqua, D. Spiller, J. Sullivan, S. D'Amico, Continuous maneuvers for spacecraft formation flying using relative orbit elements, in: Proceedings of the 9th International Workshop on Spacecraft Formation Flying, Boulder, Colorado, 2017. http://www.riccardobevilacqua.com/Di%20Mauro_ID76_v2.pdf.
[24] S. D'Amico, Autonomous Formation Flying in Low Earth Orbit, Delft University of Technology, Delft, Netherlands, 2010 Ph.D. thesis. https://repository.tudelft.nl/islandora/object/uuid:a10e2d63-399d-48e5-884b-402e9a105c70?collection=research.
[25] A.W. Koenig, T. Guffanti, S. D'Amico, New state transition matrices for spacecraft relative motion in perturbed orbits, J. Guidance Control Dyn. 40 (7) (2017) 1749–1768, doi:10.2514/1.G002409.
[26] C.W.T. Roscoe, J.J. Westphal, J.D. Griesbach, H. Schaub, Formation establishment and reconfiguration using differential elements in j2-perturbed orbits, J. Guidance Control Dyn. 38 (9) (2015) 1725–1740, doi:10.2514/1.G000999.
[27] H. Schaub, J. Junkins, Analytical Mechanics of Space Systems, American Institute of Aeronautics and Astronautics, 2003. ISBN: 9781600860270.
[28] S. D'Amico, Relative Orbital Elements as Integration Constants of Hills Equations, Technical Report, DLR, Oberpfaffenhofen, 2010. https://www.researchgate.net/publication/265495397_Relative_Orbital_Elements_as_Integration_Constants_of_Hill's_Equations.
[29] J. Sullivan, A.W. Koening, S. D'Amico, Improved maneuver free approach angles-only navigation for space rendezvous, Adv. Astronaut. Sci. Spaceflight Mech. 158 (2016). https://people.stanford.edu/damicos/sites/default/files/aassfm2016_sullivankoenigdamico.pdf.
[30] G. Gaias, J.-S. Ardaens, O. Montenbruck, Model of j2 perturbed satellite relative motion with time-varying differential drag, Celestial Mechanics and Dynamical Astronomy 123 (4) (2015) 411–433, doi:10.1007/s10569-015-9643-2.
[31] M. Farkas, Periodic Motions, Springer-Verlag, 1994. ISBN: 978-1441928382.
[32] J. Crassidis, J. Junkins, Optimal Estimation of Dynamic Systems, CRC Press, 2004. ISBN: 9780203509128 https://books.google.com/books?id=EeSQjQfJgkUC.
[33] Matworks, MathWorks, Global Optimization Toolbox: Users Guide R2017a, The MathWorks, Inc, 2017. https://www.mathworks.com/help/pdf_doc/gads/gads_tb.pdf.
[34] J.J. More, The Levenberg-Marquardt algorithm: Implementation and theory, Lecture notes in mathematics 630, ed., 1977, pp. 105–116.

[35] D. Brouwer, Solution of the problem of artificial satellite theory without drag, Astronaut. J. 64 (1963) 378–397, doi:10.1086/107958.

[36] R. Lyddane, Small eccentricities or inclinations in the brouwer theory of the artificial satellite, Astronaut. J. 68 (1963) 555–558, doi:10.1086/109179.

[37] D. Vallado, W. McClain, Fundamentals of astrodynamics and applications, Microcosm Press, 2001. ISBN: 9781881883128.